Journal of Molecular Structure 1272 (2023) 134197

Contents lists available at ScienceDirect

Journal of Molecular Structure

journal homepage: www.elsevier.com/locate/molstr

2,4-*Bis*(2,4-dimethoxyphenyl)-1,3-dithia-2,4-diphosphetane 2,4-disulfide and its derivatives: Syntheses, structural characterizations, anticancer activities, and theoretical studies on some dithiophosphonato Ni(II) complex

Ertuğrul Gazi Sağlam[a,*], Elif Bulat[a], Celal Tuğrul Zeyrek[b], Senem Akkoç[c,d], Yunus Zorlu[e], Hamza Yılmaz[f]

[a] Department of Chemistry, Marmara University, Göztepe, İstanbul 34722, Türkiye
[b] Department of Medical Services and Techniques, Çankırı Karatekin University, Çankırı 18100, Türkiye
[c] Department of Basic Pharmaceutical Science, Süleyman Demirel University, Isparta 32260, Türkiye
[d] Faculty of Engineering and Natural Sciences, Bahçeşehir University, 34353, Istanbul, Türkiye
[e] Department of Chemistry, Gebze Technical University, Kocaeli 41400, Türkiye
[f] Department of Chemistry, Ankara University, Tandoğan, Ankara 06100, Türkiye

ARTICLE INFO

Article history:
Received 5 June 2022
Revised 6 September 2022
Accepted 21 September 2022
Available online 22 September 2022

Keywords:
Perthiophosphonic acid anhydrides
2,4-diorganyl-1,3,2,4-dithiadiphosphetan-2,4-disulfide
Phosphonodithioates
Dithiophosphonates
Organodithiophosphorus compounds
Single crystal X-ray analysis
Density functional theory
Molecular docking
Antiproliferative activity
Anticancer

ABSTRACT

New 2,4-*bis*(2,4-dimethoxyphenyl)-1,3-dithia-2,4-diphosphetane 2,4-disulfide, (SAV-A2), was synthesized from the reaction P_4S_{10} and 1,3-dimethoxybenzene. SAV-A2 was reacted with alcohols to form dithiophosphonic acid monoesters (HLn, $HS_2P((2,4\text{-}CH_3O)_2C_6H_3)(ORn)$; *n*=1–3, R1=2–butyl–; R2=*n*-pentyl-; R3=*4–tert*–but-benzyl-). The acids were converted to the ammonium salts ($[NH_4Ln]$) to serve as the source of the ligands (Ln), to obtain Ni(II) complexes, ($[Ni(Ln)_2]$). $[Ni(L2)_2]$ crystal structure was elucidated by single-crystal X-ray diffraction analysis. In addition, Density Functional Theory (DFT) calculations of $[Ni(L2)_2]$ was performed. The molecular docking studies of the complex with liver cancer protein, PDB ID: 3WZE and colon cancer antigen proteins, ID 2HQ6 were done compare with experimental and theoretical results. All compounds were tested on liver- and colon cancer cell lines. Among the complexes tested, $[Ni(L3)_2]$ showed an activity closer to that of cisplatin against the colon cancer cell line. The other compounds were found to be have less active.

1. Introduction

Phosphor-1,1-dithiolates including dithiophosphate (DTP), dithiophosphinate (DTPA) and dithiophosphonate (DTPOA) ligands and their derivatives have many commercial applications such as floatation reagents in the recovery of industrial metal cations [1], as additives in lubricants [2], as pesticides in agriculture [3] and as precursors for chemical warfare [4]. They are also deemed to be a potential candidates to be used in the synthesis of antibiotics [5] and anticancoregenes against some tumors [6].

Organo-dithiophoshorus compounds have been the subject of a few studies on the field of cancer therapeutics. There are hardly any studies on the antiproliferative activities of dithiophosphinic- [7] and dithiophosphonic acids [8–10]. Anti-cancer studies with dithiophosphoric acids, on the other hand, are slightly more common [11]. Pt-dithiophosphoric acid complexes, for example, were found to be active against cancer, by Lowe et al. [12]. Cytotoxic activities of some vanadium dithiophosphates have been demonstrated by Kumar et al. in the cancers of the lung, prostate and blood [13]. So, the preliminary motives are ready to make investigations on the cancerogenic activity of dithiophosphinate and dithiophosphonate compounds.

Due to the soft-base character of dithiophosphorus-compounds, phosphor-1,1-dithiolate ligands form stable complexes with cations of soft-acid nature. There are several papers available giving the details of the synthesis, structures and chemistry, especially the metal complexes of dithiophosphorus-compounds. The

* Corresponding author.
E-mail address: egazi@marmara.edu.tr (E.G. Sağlam).

https://doi.org/10.1016/j.molstruc.2022.134197
0022-2860/

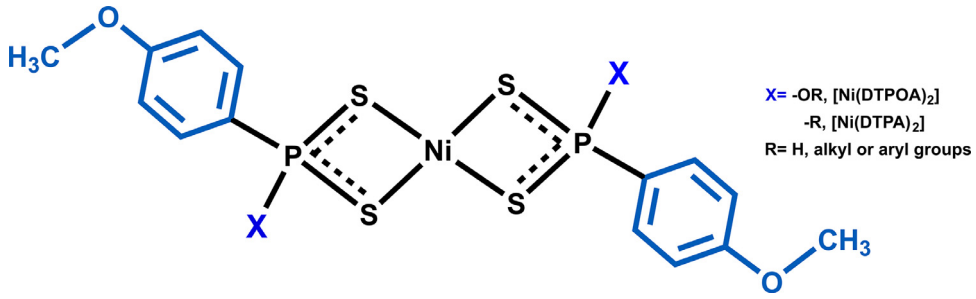

Scheme 1. Some of the organodithiophoshorus Ni(II) complexes.

metal cations that have high affinity towards dithiophosphorus-ligands tend to form four-coordinated complexes. For example, Zn(II), Cd(II) and Hg(II) are prone to form dimeric complexes with tetrahedral geometries [14,15]. Group 10 cations, Ni(II), Pd(II) and Pt(II), on the other hand, form monomeric complexes with square planar coordination geometry [15–18]. Dithiophosphonato- and dithiophosphinato complexes of Ni(II), namely $[Ni(DTPOA)_2]$ and $[Ni(DTPA)_2]$, are prepared by the direct reaction of 1,3,2,4-dithiadiphosphetane 2,4-disulfides (Lawesson reagent, (LR), for example), with an monofunctional alcohol, ROH [19] or with a Grignard reagent, R-MgX [20], respectively (Scheme 1).

1,3,2,4-dithiadiphosphetane 2,4-disulfides are the most valuable cyclic phosphorus-sulfur compounds that are also named perthiophosphonic acid anhydrides. They are depicted by the general formula $(PR_2S)_2$, (*R*= alkyl-, aryl-). The most common commercial representative of this class is LR with *R*=(4-CH_3O)Ph- [21]. Belleau reagent (*R*=PhOPh-) [22], Davy reagent (R=CH_3S-) [23], Ferrocenyl Lawesson reagent (R=Cp-) [24] and Yokoyama reagent (*R*=PhS-) [25] are the other perthiophosphonic acid anhydrides. In recent years, LR analog as SAV-B1 (*R*=(4-CH_3O)(2-CH_3)Ph-) and SAV-B2, (*R* = 1-CH_3O)(2-CH_3)Ph-) were reported to have been prepared [26].

Here, we report the preparation of another diphosphetane 2,4-disulfide (Scheme 2A), namely, 2,4-*bis*(2,4-dimethoxyphenyl)−1,3-dithia-2,4-diphosphetane 2,4-disulfide, (SAV-A2). This compound was reacted with alcohols to prepare the compounds, $HS_2P((2,4\text{-}CH_3O)_2C_6H_3)$(ORn); R1=2–butyl–; R2=*n*-pentyl-; R3=4–*tert*-butylbenzyl- (Scheme 2B). The compounds are collectively denoted by HLn (Scheme 2C). The acids, HLn, were converted to ammonium dithiophosphonate salts, $[NH_4Ln]$ for purification and later use as the source of the dithiophosphonate ligands (Scheme 2D). Dithiophosphonato-Ni(II) complexes, $[Ni(Ln)_2]$, were prepared by the action of the ammonium salts on an ethanol - solution of $NiCl_2$ (Scheme 2E).

The compounds were characterized by FT-IR, mass spectrometry and multinuclear NMR spectroscopy. The crystal structure of $[Ni(L2)_2]$ was elucidated by single crystal X-ray diffraction technique. Ligands and their Ni(II) complexes were used for anticancer studies. The Density Functional Theory (DFT) calculations for the ground state of the complex $[Ni(L2)_2]$ have been performed using the B3LYP/LANL2DZ/6–31+*G*(d,p) level program, and the optimized geometry was compared with that found by single crystal X-ray diffraction analysis of the same compound. The energy levels, the orientation of the frontier molecular orbitals (HOMOs and LUMOs), molecular potential surfaces (MEPs) and the chemical parameters of the complex have been determined by DFT in the gas phase. The interactions of the complex $[Ni(L2)_2]$ with DNA samples were predicted and the results found were compared with experimental activity data. Within this context, the molecular docking studies of $[Ni(L2)_2]$ with liver cancer protein (PDB ID: 3WZE) and colon cancer antigen protein (PDB ID: ID 2HQ6) were investigated.

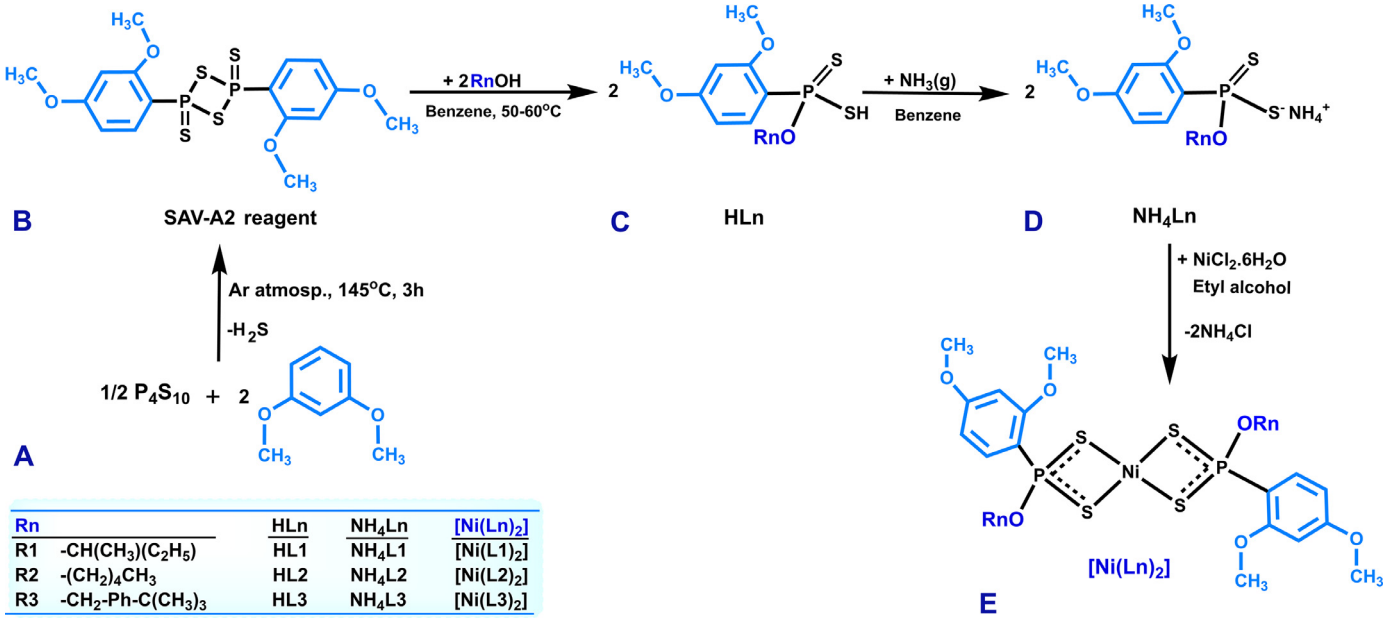

Rn		HLn	NH_4Ln	$[Ni(Ln)_2]$
R1	-$CH(CH_3)(C_2H_5)$	HL1	NH_4L1	$[Ni(L1)_2]$
R2	-$(CH_2)_4CH_3$	HL2	NH_4L2	$[Ni(L2)_2]$
R3	-CH_2-Ph-$C(CH_3)_3$	HL3	NH_4L3	$[Ni(L3)_2]$

Scheme 2. The syntheses reaction of the compounds.

Table 1
Crystal data and structure refinement details for $[Ni(L2)_2]$.

Compound	$[Ni(L2)_2]$
CCDC	2,054,970
The formula of Refinement Model	$C_{26}H_{40}NiO_6P_2S_4$
Formula weight	697.47
Temperature/K	173
Radiation, Wavelength (Å)	MoKα (λ = 0.71073)
Crystal system	Triclinic
Space group	*P-1*
a/Å	7.7485(11)
b/Å	7.9589(12)
c/Å	13.793(2)
α/°	105.315(2)
β/°	99.061(2)
γ/°	91.880(2)
Crystal size/mm^3	0.52 × 0.50 × 0.23
Volume/Å^3	807.7(2)
Z	1
ρ_{calc}g/cm^3	1.434
μ/mm^{-1})	0.995
F(000)	366
2θ range for data collection/°	3.108 to 50
Index ranges	$-9 \le h \le 9$, $-9 \le k \le 9$, $-16 \le l \le 16$
Reflections collected	9941
Independent reflections	2851 [R_{int} = 0.0260, R_{sigma} = 0.0222]
Data/restraints/parameters	2851/0/181
Goodness-of-fit on F^2 (S)	1.039
Final R indices [$I > 2\sigma(I)$]	R_1 = 0.0232, wR_2 = 0.0612
R indices (all data)	R_1 = 0.0244, wR_2 = 0.0619
Largest diff. peak/hole / e Å^{-3}	0.35/−0.26

2. Experimental

2.1. Materials and instruments

Ethanol, 2–butyl alcohol *n*-pentyl alcohol, 4–*tert*-butylbenzyl alcohol, 1,3-dimethoxybenzene, P_4S_{10}, $NiCl_2{\cdot}6H_2O$, benzene, chloroform and diethyl ether were purchased from Sigma-Aldrich.

The LC/MS system was supplied by Waters with a C-18 HPLC column and a Waters Micromass ZQ connected to an ESI ionizer. Melting point determinations were done on a Gallenkamp apparatus with a glass capillary. ^{1}H (500 MHz), ^{13}C (^{1}H decoupled; 125 MHz) and ^{31}P NMR (^{1}H decoupled; 202.4 MHz) spectra were recorded on a Bruker FT spectrometer at 298 K. ^{1}H and ^{13}C NMR chemical shifts (δ) are given in ppm and referenced to the internal signal of TMS. 85% H_3PO_4 was used as the external standard for ^{31}P NMR. D_2O was the solvent of choice for $[NH_4Ln]$ and $CDCl_3$ for $[Ni(Ln)_2]$ complexes. Diagnostic correlations which are based on Hetero Nuclear Single Quantum Coherence (HSQC) experiments were also performed on a Bruker FT spectrometer at 298 K. IR spectra were recorded on a Perkin Elmer Spectrum 400 FT-IR instrument (200–4000 cm^{-1}) with wavenumbers in cm^{-1} units. Elemental analyses were performed on a LECO CHNS-932 C instrument.

Table 2
The predicted bonding energies and RMSD values as a consequence of molecular docking for $[Ni(L2)_2]$ by using AutoDock-Vina software.

Complex 3WZE, 2HQ6	Mode	Affinity (kcal/mol)	Distance from the best mode	
			RMSD l.b.	RMSD u.b.
$[Ni(L2)_2]$−3WZE	1	−7.3	0.000	0.000
	2	−7.1	1.330	11.481
	3	−7.1	1.239	2.137
	4	−6.9	2.425	9.777
	5	−6.9	2.853	7.008
	6	−6.7	2.798	7.222
	7	−6.7	3.220	7.605
	8	−6.4	2.987	9.285
	9	−6.4	3.198	9.127
$[Ni(L2)_2]$−2HQ6	1	−6.0	0.000	0.000
	2	−5.8	1.608	11.182
	3	−5.8	0.554	11.266
	4	−5.8	1.863	2.562
	5	−5.2	2.206	10.963
	6	−5.0	3.223	4.214
	7	−5.0	5.454	11.593
	8	−4.8	3.806	11.220
	9	−4.7	3.427	11.131

2.2. Synthesis

2.2.1. Preparation of the 2,4-bis(2,4-dimethoxyphenyl)−1,3-dithia-2,4-diphosphetane 2,4-disulfide, (SAV-A2)

In a 145 °C oil-bath under a fume hood, 1,3-dimetoxybenzene (4.97 g, 35.96 mmol) was added dropwise, with constant stirring, onto a P_4S_{10} sample (4 g, 8.99 mmol) in a round-bottom flask while passing Ar gasses to provide an inert atmosphere. The mixture turned into a clear, pale-yellow solution in about 1 hour after the dropwise addition step. The stirring procedure was continued and a yellow precipitate started to form in 2 h. After 3 h, the mixture was taken out of the oil bath and left aside for cooling to room temperature. A deep yellow solid was formed at the bottom of the flask. The solid was filtered; washed with dry diethyl ether and then crushed in ether medium with a spatula. The ether-washed solid was filtered again and dried in an inert (Ar) atmosphere. Our experience is that the yellow product decomposes in 1 hour under humid atmosphere.

2.2.2. General procedure for the ammonium salts of dithiophosphonic acids [NH_4Ln]

2.00 g (4.30 mmol) of the SAV-A2 reagent was taken into a three-necked flask, and onto it, an 8.60 mmol of one of the alco-

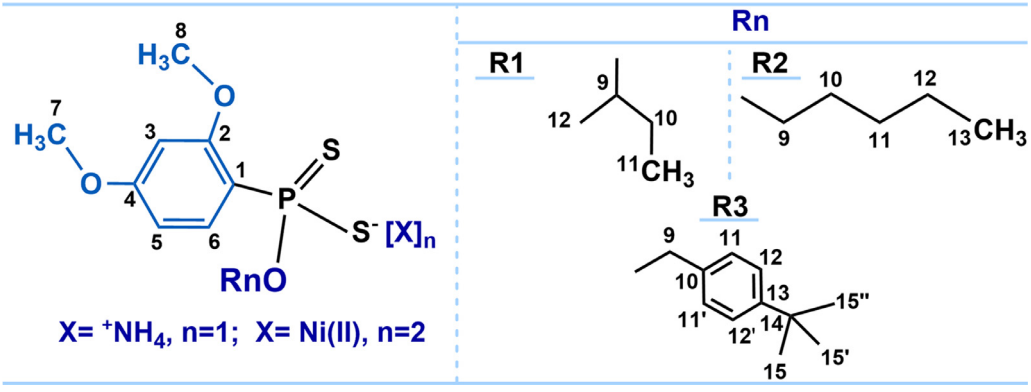

Fig. 1. The numbering scheme for ligands and complexes.

Table 3
^{1}H NMR data of the compounds . (D_2O for $[NH_4Ln]$, $CDCl_3$ for $[Ni(Ln)_2]$; δ in ppm, J in Hz, s: *singlet*, d: *doublet*, dd: *doublet of doublets*, t: *triplet*, and m: *multiplet*).

	$[NH_4L1]$	$[NH_4L2]$	$[NH_4L3]$	$[Ni(L1)_2]$	$[Ni(L2)_2]$	$[Ni(L3)_2]$
C_3-*H*	6.6 (m, 2H)	6.6 (m, 2H)	6.5 (m, 2H)	6.4 (s, 2H)	6.4 (d, 2H); $^{4}J_{PH}$= 3.4	6.4 (d, 2H); $^{3}J_{PH}$= 3.5
C_5-*H*	C_3H is adjacent to C_5H	C_3H is adjacent to C_5H	C_3-*H* is adjacent to C_5H	6.6 (d, 2H); $^{3}J_{HH}$=8.0	6.6 (d, 2H); $^{3}J_{HH}$=8.5	6.6 (d, 2H); $^{3}J_{HH}$=8.6
C_6-*H*	8.1 (dd, H)	8.1 (dd, H)	8.2 (dd, H)	8.0 (dd, 2H)	7.9 (dd, 2H)	7.9 (dd, 2H)
	$^{3}J_{PH}$= 17.0; $^{3}J_{HH}$= 8.4	$^{3}J_{PH}$= 16.7;$^{3}J_{HH}$= 8.7	$^{3}J_{PH}$= 16.6; $^{3}J_{HH}$= 8.5	$^{3}J_{PH}$= 17.7; $^{3}J_{HH}$= 8.2	$^{3}J_{PH}$= 17.9; $^{3}J_{HH}$= 8.6	$^{3}J_{PH}$= 18.1; $^{3}J_{HH}$= 8.6
C_7-*H*	3.9 (s, 6H)	3.8 (s, 3H)	3.8 (s, 6H)	3.9 (s, 6H)	3.9 (s, 6H)	3.8 (s, 12H)
C_8-*H*		3.9 (s, 3H)		3.8 (s, 6H)	3.8 (s, 6H)	
C_9-*H*	4.5 (m, H)	3.8 (dd, 2H)	4.9 (d, 2H); $^{3}J_{PH}$= 8.8	4.9 (m, 2H)	4.3 (dd, 4H)	5.3 (d, 4H); $^{3}J_{PH}$= 9.5
		$^{3}J_{PH}$= 15.5;$^{3}J_{HH}$= 6.8			$^{3}J_{PH}$= 15.8; $^{3}J_{HH}$= 6.4	
C_{10}-*H*	1.6 (m, 2H)	1.6 (m, 2H)	–	1.6 (m, 4H)	1.7 (m, 4H)	–
C_{11}-*H*	0.9 (t, 3H); $^{3}J_{HH}$= 7.5	–	–	1.0 (t, 6H); $^{3}J_{HH}$= 6.8	–	–
C_{12}-*H*	1.2 (d, 3H); $^{3}J_{HH}$= 6.3	–	–	1.4 (d, 6H); $^{3}J_{HH}$= 5.6	–	–
C_{13}-*H*	–	0.8 (t, 3H); $^{3}J_{HH}$= 7.0	–	–	0.9 (t, 6H); $^{3}J_{HH}$= 6.3	–
C_{15}-*H*	–	–	1.3 (s, 9H)	–	–	1.3 (s, 18H)
$C_{11,12}$-*H*	–	1.3 (m, 4H)	7.3 (s, 4H)	–	1.4 (s, 8H)	7.4 (s, 8H)

Table 4
^{13}C NMR data of the compounds. (D_2O for $[NH_4Ln]$, $CDCl_3$ for $[Ni(Ln)_2]$; δ in ppm, J in Hz).

	$[NH_4L1]$	$[NH_4L2]$	$[NH_4L3]$	$[Ni(L1)_2]$	$[Ni(L2)_2]$	$[Ni(L3)_2]$
C_1	124.3, J_{PC}= 114.0	123.3, J_{PC}= 111.0	125.9 superimposed with $C_{11,11'}$	116.5, J_{PC}= 118.1	116.1, J_{PC}= 116.8	115.7, J_{PC}= 116.5
C_2	163.7, $^{2}J_{PC}$= 3.6	163.5, $^{2}J_{PC}$= 3.6	162.6, $^{2}J_{PC}$= 3.3	161.8	162.0	162.0
C_3	101.6, $^{3}J_{PC}$= 7.9	101.5, $^{3}J_{PC}$= 7.8	99.5, $^{3}J_{PC}$= 7.7	99.0, $^{3}J_{PC}$= 7.8	99.0, $^{3}J_{PC}$= 7.9	99.0, $^{3}J_{PC}$= 8.0
C_4	166.0, $^{4}J_{PC}$=2.8	166.0, $^{4}J_{PC}$= 2.9	164.8, $^{4}J_{PC}$= 2.1	164.9	164.9	165.1
C_5	107.1, $^{3}J_{PC}$= 15.0	107.2, $^{3}J_{PC}$= 14.8	107.2, $^{3}J_{PC}$= 14.8	104.3, $^{3}J_{PC}$= 18.1	104.3, $^{3}J_{PC}$= 16.9	104.4, $^{3}J_{PC}$= 16.8
C_6	137.6, $^{2}J_{PC}$= 13.0	137.8, $^{2}J_{PC}$= 12.7	136.5, $^{2}J_{PC}$= 12.3	134.3, $^{2}J_{PC}$= 15.3	134.2, $^{2}J_{PC}$= 14.6	134.3, $^{2}J_{PC}$= 14.8
C_7	58.4	58.4	55.8	55.6	55.8	55.8
C_8	58.0	58.2			55.6	55.6
C_9	78.2, $^{2}J_{PC}$= 7.9	68.4, $^{2}J_{PC}$= 7.9	66.9, $^{2}J_{PC}$= 6.0	76.2	66.3, $^{2}J_{PC}$= 6.2	67.3, $^{2}J_{PC}$= 5.5
C_{10}	32.8, $^{3}J_{PC}$= 4.6	32.2, $^{3}J_{PC}$= 8.5	137.0, $^{3}J_{PC}$= 9.8	30.5	29.9, $^{3}J_{PC}$= 7.5	133.3, $^{3}J_{PC}$= 9.2
C_{11}	11.7	30.2	125.9 superimposed with C_1	21.8	27.7	125.3
C_{12}	23.0, $^{3}J_{PC}$= 3.3	24.5	128.9	9.5	22.2	127.9
C_{13}	–	16.2	151.3	–	14.0	151.1
C_{14}	–	–	35.3	–	-	34.6
C_{15}	–	–	31.8	–	-	31.3

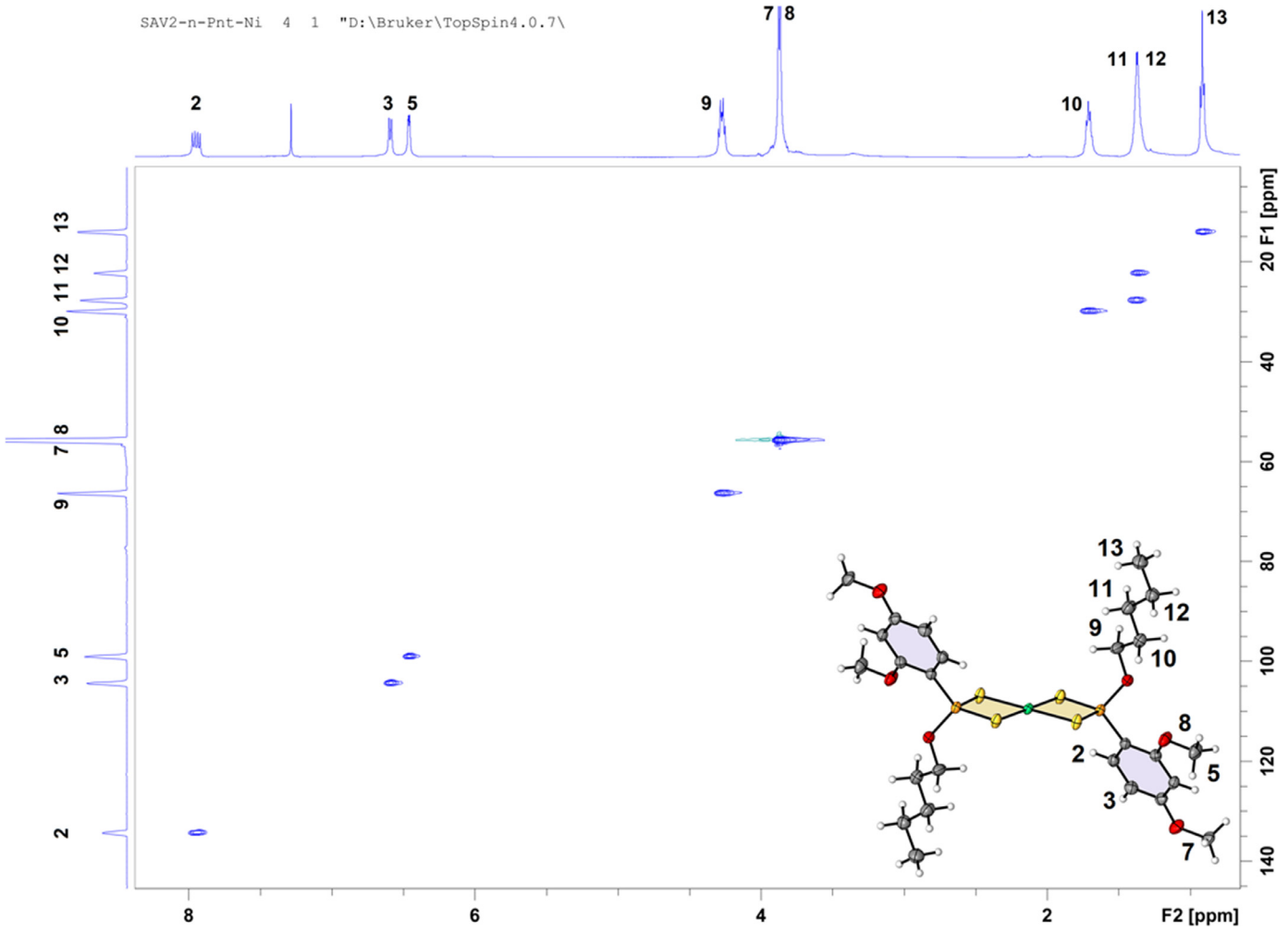

Fig. 2. HSQC spectrum of [Ni(L2)$_2$].

hols (0.64 g of 2–butyl alcohol; 0.76 g of *n*-pentyl alcohol; 1.41 g of 4–*tert*-butylbenzyl alcohol) was added dropwise. The mixture was heated to 50–60 °C, kept at this temperature range until complete dissolution and then left aside to cool. The crude dithiophosphonic acid (an oily, viscous mixture), was poured into 50–60 mL of benzene. The benzene solution was filtered (filter paper) and was cooled to 0 °C. Through this solution dry ammonia gas was bubbled at a rate of 20 mL/min until the precipitation was complete. The white, amorphous precipitate ([NH_4Ln]) was filtered (filter paper), washed with benzene and dried in a vacuum desiccator.

2.2.3. General procedure for the synthesis of the complexes [Ni(Ln)$_2$]

4.21 mmol sample of the ammonium salt interested (1.36 g of [NH_4L1]; 1.42 g of [NH_4L2]; 1.74 g of [NH_4L3]) was dissolved in 30–40 mL ethanol. Onto this, a solution of 2,10 mmol (0.5 g) $NiCl_2{\cdot}6H_2O$ in the same solvent was added dropwise. The mixture was heated to 50–60 °C; kept as such for 5–10 min and filtered through filter paper without letting excess cooling. Tiny, violet crystals form upon cooling. This compound was recrystallized from ethanol or chloroform.

Experimental details for compounds are follows:

SAV-A2: Yield: 3.01 g (72%). Yellow. M.P.: 92 °C. Anal. Calcd. for: $C_{16}H_{18}O_4P_2S_4$ (464.52 g.mol^{-1}): C, 41.37; H, 3.91; S, 27.61; found: C, 41.40; H, 3.95; S, 27.64%.

[NH_4L1]: Yield: 1.98 g (71%). White. M.P.:167–168 °C. ^{31}P NMR: δ=99.8. LC/MS: *m/z* 351.9 ([(M-NH_4)(E*t*OH]$^+$, 100%). Anal. Calcd. for: $C_{12}H_{22}NO_3PS_2$ (323.41 g.mol^{-1}): C, 44.56; H, 6.86; N, 4.33; S, 19.83; found: C, 44.66; H, 6.96; N, 4.42; S, 19.90%.

[NH_4L2]: Yield: 2.15 g (73%). White. M.P.: 178 °C. ^{31}P NMR: δ=102.3. LC/MS: *m/z* 365.8 ([(M-NH_4)(E*t*OH]$^+$, 100%). Anal. Calcd. for: $C_{13}H_{24}NO_3PS_2$ (337.44 g.mol^{-1}): C, 46.27; H, 7.17; N, 4.15; S, 19.00; found: C, 46.40; H, 7.30; N, 4.27; S, 19.12%.

[NH_4L3]: Yield: 2.63 g (73%). White. M.P.:187–188 °C. ^{31}P NMR: δ=103.4. LC/MS: *m/z* 442.0 ([(M-NH_4)(E*t*OH]$^+$, 100%). Anal. Calcd. for: $C_{19}H_{28}NO_3PS_2$ (413.53 g.mol^{-1}): C, 55.18; H, 6.82; N, 3.39; S, 15.51; found: C, 55.21; H, 6.84; N, 3.43; S, 15.57%.

[N*i*(L1)$_2$]: Yield: 0.98 g (70%). Violet. M.P.:167 °C. ^{31}P NMR: δ=98.5. LC/MS: *m/z* 670.1 ([*M*+*H*]$^+$, 100%). Anal. Calcd. for: $C_{23}H_{36}NiO_6P_2S_4$ (669.44 g.mol^{-1}): C, 43.06; H, 5.42; S, 19.16; found: C, 43.14; H, 5.50; S, 19.24%.

[N*i*(L2)$_2$]: Yield: 1.28 g (87%). Violet. M.P.:107 °C. ^{31}P NMR: δ=101.4. LC/MS: *m/z* 698.2 ([*M*+*H*]$^+$, 100%). Anal. Calcd. for: $C_{26}H_{40}NiO_6P_2S_4$ (697.49 g.mol-1): C, 44.77; H, 5.78; S, 18.39; found: C, 44.89; H, 5.90; S, 18.51%.

[N*i*(L3)$_2$]: Yield: 1.32 g (74%). Violet. M.P.:179 °C. ^{31}P NMR: δ=102.6. LC/MS: *m/z* 185.6 ([N*i*S$_4$]$^+$, 100%), 850.27 ([*M*+*H*]$^+$, 82%). Anal. Calcd. for: $C_{38}H_{48}NiO_6P_2S_4$ (849.69 g.mol^{-1}): C, 53.71; H, 5.69; S, 15.10; found: C, 53.71; H, 5.74; S, 15.15%.

2.3. X-ray data collection and structure refinement of [Ni(L2)$_2$]

Single crystal data for [Ni(L2)$_2$] were obtained with Bruker APEX II QUAZAR three-circle diffractometer. Indexing was per-

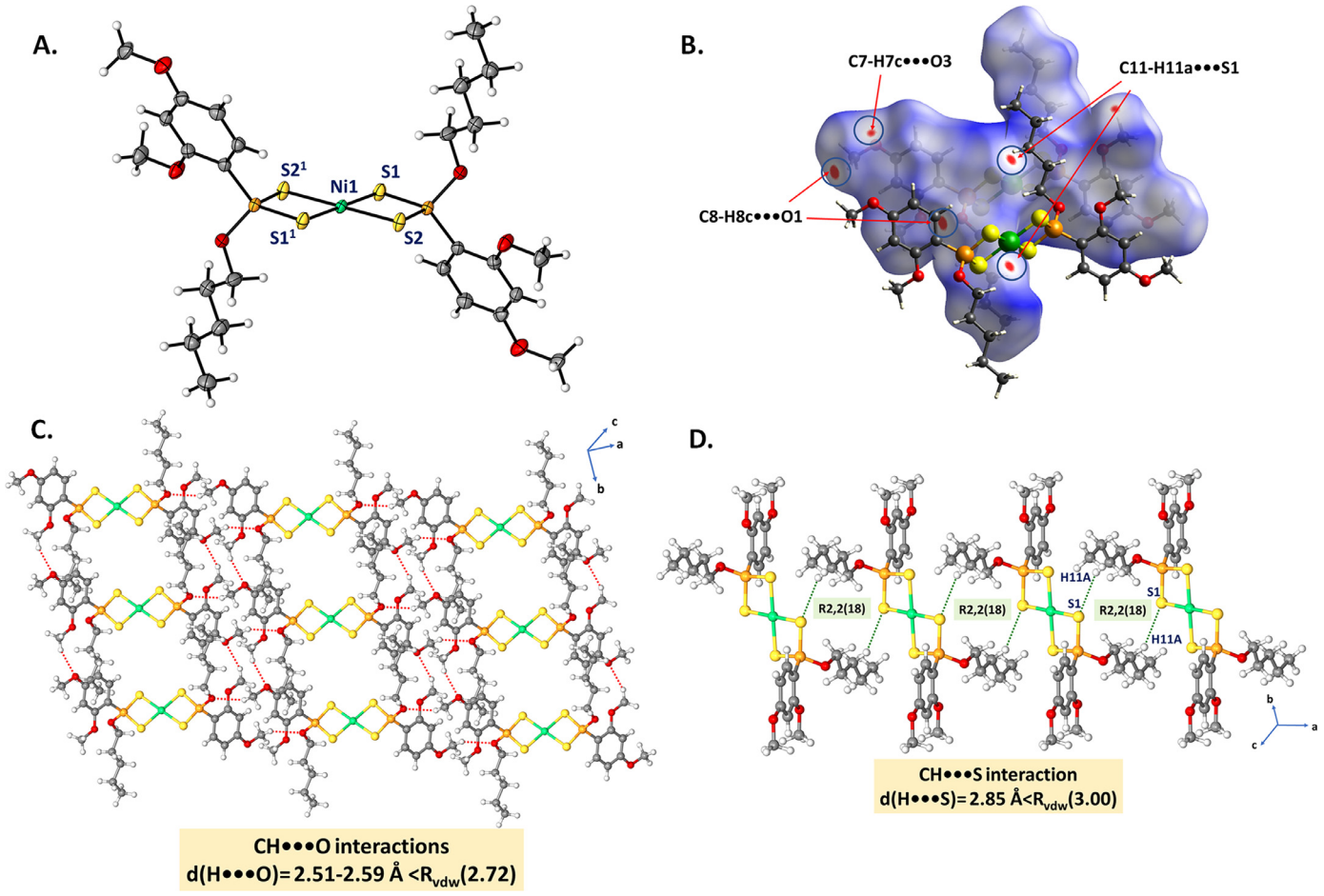

Fig. 3. A. A view of the structure of $[Ni(L2)_2]$, showing the atom-labeling scheme. Displacement ellipsoids are drawn at the 50% probability level. Symmetry code: (a) 2 − x,1 − y, 2 − z. **B.** HS of $[Ni(L2)_2]$ mapped with d_{norm}, showing the C—H···O (red dotted lines) and C—H···S (green dotted lines) hydrogen bonding interactions. **C.** Perspective view of the 2D constructed from the C—H···O hydrogen bonds. **D.** The 1D chains constructed from the hydrogen bonding rings with R2,2(18)-graph-set notation.

formed using APEX2 [27]. Data indexing, integration and reduction were performed with Bruker SAINT [28]. Absorption correction was performed by the multi-scan method implemented in Bruker SADABS [29]. $[Ni(L2)_2]$ was solved using SHELXT [30] and then refined by full-matrix least-squares refinements on F^2 using the SHELXL [31] in Olex2 software package [32]. The positions of all hydrogen atoms which were bonded to carbon were geometrically optimized with the following HFIX instructions in SHELXL: HFIX 137 for the -CH_3, HFIX 23 for the –CH_2, and HFIX 43 for the CH of the aromatic rings. Finally, their displacement parameters were set to isotropic thermal displacements parameters ($U_{iso}(H) = 1.2 \times U_{eq}$ for $CH_{aromatic}$, CH_2 and ($U_{iso}(H) = 1.5 \times U_{eq}$ (CH_3 groups). Crystallographic data and refinement details of the data collection for $[Ni(L2)_2]$ are given in Table 1. Crystal structure validations and geometrical calculations were performed using Platon software [33]. Mercury software [34] was applied for the cif files visualization.

2.4. Computational methods

2.4.1. DFT calculations

The DFT calculations of the complex $[Ni(L2)_2]$ were performed by the Gaussian 09 software package and the Gauss-view visualization program [35]. The single crystal X-ray diffraction experimental data of $[Ni(L2)_2]$ were used to prepare the input file for the geometry in Gaussian. The complex was optimized at B3LYP/LANL2DZ/6–31+*G*(d,p) level in ground state [36–38] used in DFT calculation to predict the geometry optimizations, total energies, HOMO and LUMO orbitals and MEP surfaces of the compound.

2.4.2. Molecular docking calculations

The molecular docking calculations of $[Ni(L2)_2]$ with liver cancer protein, PDB ID: 3WZE and colon cancer antigen proteins, ID 2HQ6 to predict the interaction mechanism were performed by using AutoDock-Vina software [39]. 3D molecular structures of the proteins were obtained from Protein Data Bank (PDB). All residues were removed and then polar hydrogens were added to produce favorable protonation states for molecular docking using Discover Studio Visualizer 4.0 software [40]. AutoDockTools (ADT) was used for creating docking data entry files [41]. ADT was performed to add partial charges using the Geistener method and to define torsions and rotatable bonds. The active sites of the proteins were defined to include residues of the active site within the grid size of 30 × 30 × 30 Å. To evaluate the quality of docking results, it is common to calculate the Root Mean Square Deviation (RMSD) between the docked pose and the known crystal structure confirmation. Docking results are acceptable when the RMSD value is lower than 2 Å [42]. At the same time, between molecular docking executions were performed, the most favorable ones being represented by the lowest free-bond energy (ΔG) [43]. The predicted bonding energies and RMSD values as a consequence of molecular docking for $[Ni(L2)_2]$ are listed in Table 2. The interactions figures were drafted using Discover Studio Visualizer 4.0 software [40].

2.4.3. In vitro *cytotoxic activity studies*

Human colon cancer cell line (DLD-1) (ATCC® CCL-221™) and human liver hepatocellular carcinoma cell line (HepG2) (ATCC®

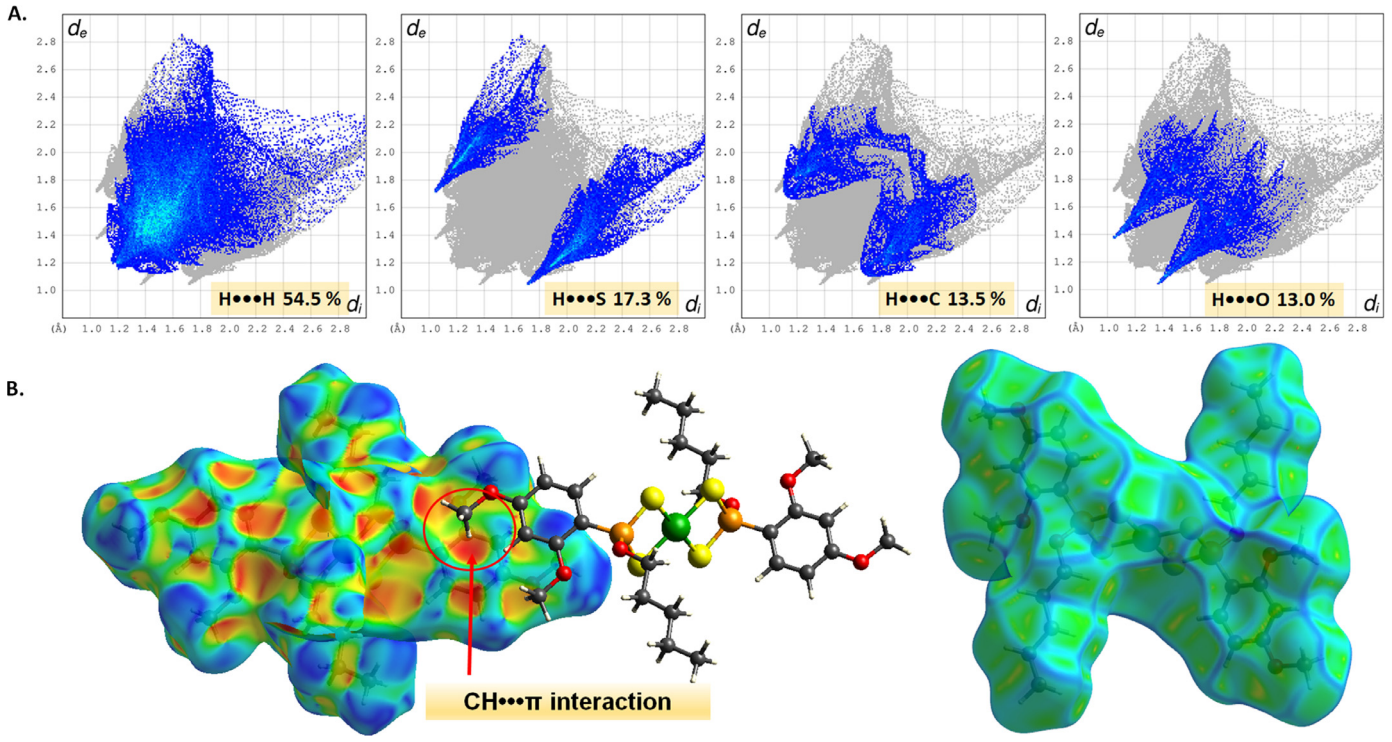

Fig. 4. A. The resolved 2D fingerprint plots showing the percentage contributions to the total HS area. **B.** HS mapped with shape index (left) and curvedness (right) of $[Ni(L2)_2]$. The HS shape index exhibits concave curvature, where C—H···π interaction occurs.

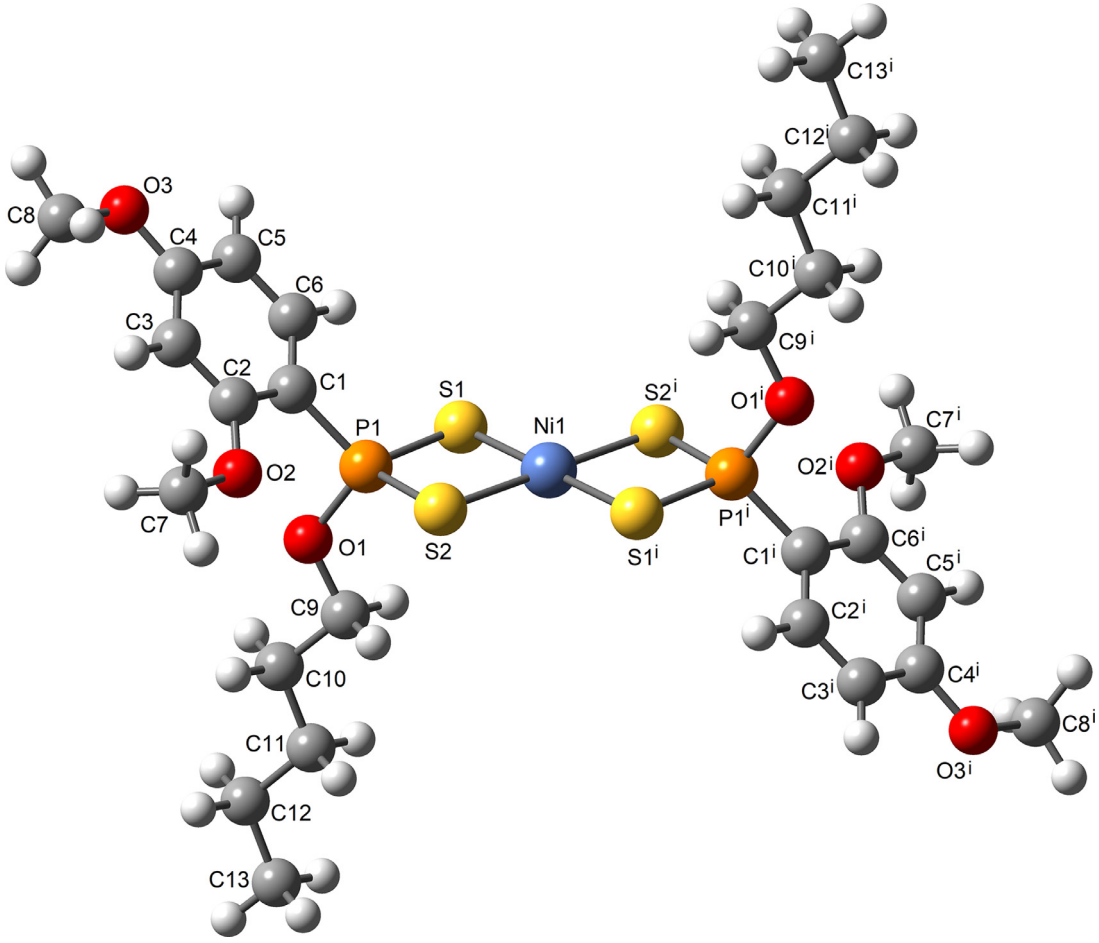

Fig. 5. The optimized structures of the complex $[Ni(L2)_2]$ by DFT.

Table 5
The intermolecular C—H···X (X = O, S, π) interactions (Å and °) for [Ni(L2)$_2$].

D—H···A	Symmetry	d(D—H)	d(H···A)	d(D—H···A)	D—H···A
C8—H8C···O1	2656.01	0.98	2.51	3.347	142.99
C7—H7C···O3	1565.01	0.98	2.59	3.325	131.87
C11—H11A···S1	2667.01	0.99	2.85	3.739	149.23
C8—H8B···Cg2	2756.01	0.98	2.77	3.631	146.47

Represents the ring built up by atoms C1-C2-C3-C4-C5-C6.

HB-8065^{TM}) were purchased from American Type Culture Collection (ATCC, USA).

The cytotoxic activity studies were done according to the literature procedures [44,45]. The DLD-1 and HepG2 cells were seeded into sterile 96-well plates at a density of 5.10^3 cells/well. After 24 h, cells were exposed to compounds at six different concentrations for 48 h. After this period was completed, 5 mg/mL of MTT stock solution was added to each well, and the plates were incubated for 2 h. The measure of absorbance values was done using the Promega plate reader device at 560 nm. IC_{50} values were calculated using GraphPad Prism software 5.

3. Result and discussion

3.1. Spectroscopic studies

The characteristic ν(N-H) stretching bands of the ligands appear at 2967–2953 cm^{-1} on IR. These bands disappear on the IR spectra of the complexes proving the substitution of the ammonium group by metal cations. Symmetric and asymmetric PS stretching vibrations ($\nu(PS)_{sym}$ and $\nu(PS)_{asym}$) of the ligands are shown up at 559–554 cm^{-1} cm^{-1} and 665–651 cm^{-1}, respectively. On the other hand, the spectra of the complexes all show two bands in the ranges 560–549 cm^{-1} and 682–669 cm^{-1} attributable to the ν_{sym} and ν_{asym} PS stretching bands, respectively. The complexes also display Ni-S bands ($\nu(Ni\text{-}S)_{sym}$ and $\nu(Ni\text{-}S)_{asym}$) that are located at 271–287 cm^{-1} and 330–342 cm^{-1}, respectively. IR data reported for similar compounds agree well with our findings [18,26,46,47].

All the ligands and complexes display intense molecular ion peaks. The ammonium salts display the corresponding dithiophosphonic acids as the molecular ion. In the section, experimental, we represent the molecular ions by [M-NH$_4$]$^+$. In general, all the [M-NH$_4$]$^+$ species are accompanied by one molecule of EtOH. These peaks are the most intense (principal) ones on all the MS spectra. The molecular ion peaks of the complexes, $[M+H]^+$, are also the principal peak, except for [Ni(L3)$_2$].

The starting material, SAV-A2, is insoluble in the common NMR solvents, so no NMR data were provided for it. The numbering system used for assignments of the protons is also given in Fig. 1.

The ^{1}H NMR data is given in Table 3. In the ^{1}H NMR spectra of all the compounds tested, the C_6-***H*** proton on the 2,4-dimethoxyphenyl ring appears as a doublet of doublets indicating splittings by the phosphorus ($^3J_{PH}$= 16.6–17.0 Hz for the ligands and $^3J_{PH}$= 17.7–18.1 Hz for the complexes) and also by C_5-***H*** proton ($^3J_{HH}$= 8.4–8.7 Hz for the ligands and $^3J_{HH}$= 8.2–8.6 Hz for the complexes). The methoxy protons C_7-***H*** and C_8-***H*** on the aromatic moiety were overlapped. The chemical shifts of the methoxy protons are δ=~3.8–3.9 ppm in ligands and complexes.

The signals of the C_3-***H*** and C_5-***H*** protons are adjacent to each other for the ligands. These protons are somewhat (C_3-***H***; $^4J_{PH}$= 3.4–3.5 Hz, C_5-***H***; $^3J_{HH}$=8.0–8.6 Hz) separated from each other in the spectra of the complexes. On the spectra of the ligand [NH$_4$L2], the P-O-C_9-***H*** proton is very close to O-C***H***$_3$ (attached to the aromatic ring) protons. But more distant on that of the complex; obviously because the aromatic ring O-C***H***$_3$ protons are effected by complexation.

As given in Table 4, on the ^{13}C NMR spectra of the ligands, the signals of the neighboring carbons $\boldsymbol{C}_5$ and $\boldsymbol{C}_6$ are split by the phosphorus in the ranges reported [26] for the two-bond P-***C*** coupling ($^2J_{PC}$= 12.3–13.0 Hz) and the three-bond P-***C*** coupling ($^3J_{PC}$= 14.8–15.0 Hz), respectively. As is the case in many similar structures, the three-bond P-***C*** coupling displayed by the nuclei $\boldsymbol{C}_5$ ($^3J_{PC}$= 14.8–15.0 Hz) is higher than the two-bond couplings of $\boldsymbol{C}_6$ ($^2J_{PC}$= 12.3–13.0 Hz).

Similar cases in the coupling patterns of the 2,4-dimethoxyphenyl ring protons are reflected in the ^{13}C NMR spectra of the complexes.

^{31}P-NMR spectra of the [NH$_4$Ln] are of single peaks and ^{31}P chemical shifts of the ligands are observed in the range 99.8–103.4 ppm and those of the complexes in the range 98.5–102.6 ppm.

Table 6
Selected experimental and calculated [B3LYP/LANL2DZ/6–31+*G*(d,p) level in the ground state] bond lengths (Å), bond angles (°) and torsion angles for [Ni(L2)$_2$].

Bond lengths (Å)			Bond angles (°)		
	X-ray	Calculated		X-ray	Calculated
Ni1—S1	2.222(2)	2.3506	S1—Ni1—S1^i	180.0	180.0
Ni1—S2	2.241(2)	2.3490	S2^i—Ni1—S2	180.0	180.0
S1—P1	2.004(2)	2.1947	S2—Ni1—S1^i	92.07(2)	90.247
S2—P1	2.009(2)	2.1926	S1—Ni1—S2	92.07(2)	90.247
P1—O1	1.582(2)	1.6231	P1—S1—Ni1	87.93(2)	85.983
P1—C1	1.790(2)	1.8376	P1—S2—Ni1	87.93(2)	86.071
O1—C9	1.462(2)	1.4798	S2—P1—S1	101.08(2)	98.193
O2—C2	1.359(2)	1.3843	O1—P1—S1	113.02(2)	111.988
O2—C7	1.432(2)	1.4563	O1—P1—S2	113.14(2)	113.539
O3—C4	1.359(2)	1.3899			
O3—C8	1.435(2)	1.4576			
Torsion angles (°)					
	X-ray	Calculated		X-ray	Calculated
S1—P1—O1—C9	61.6(1)	60.018	P1—O1—C9—C10	122.6(1)	179.466
S1—P1—C1—C2	176.1(1)	−171.223	P1—C1—C2—O2	−1.3(2)	0.728
S1—P1—C1—C6	−7.8(1)	8.758	O1—P1—C1—C2	54.8(1)	−68.518
S2—P1—O1—C9	−52.5(1)	50.073	O1—P1—C1—C6	−129.0(1)	−111.501
S2—P1—C1—C2	−68.4(1)	−56.791	O2—C2—C3—C4	176.1(2)	179.637
S2—P1—C1—C6	107.7(2)	123.190	C1—P1—O1—C9	−177.6(1)	−178.833

Table 7
Calculated total energies, dipole moments and chemical parameters of the compounds $[Ni(L2)_2]$.

Parameters	$[Ni(L2)_2]$	
E_{TOTAL}(Hartee)	−1688.7629	E_{TOTAL}: Total energy
E_{HOMO} (eV)	−5.9226	E_{HOMO} and E_{LUMO}: Energy values of HOMO and LUMO
E_{LUMO} (eV)	0.1442	$\Delta E_{Gap} = (E_{LUMO} - E_{HOMO})$: Gap of energy.
ΔE_{Gap}(eV)	6.0668	I: Ionization potential.
I (eV)	5.9226	A: Electron affinity.
A(eV)	−0.1442	η: Absolute hardness. $(I\text{-}A)/2$.
η (eV)	3.0334	χ: Electronegativity. $(I + A)/2$.
χ (eV)	2.8892	σ: Softness. $1/\eta$.
σ (eV)	0.3297	μ_p: Chemical potential. $-(I + A)/2$
μ_p(eV)	−2.8892	ω:Electrophilicity.$\mu_p^2/2\eta$.
ω	12.6603	

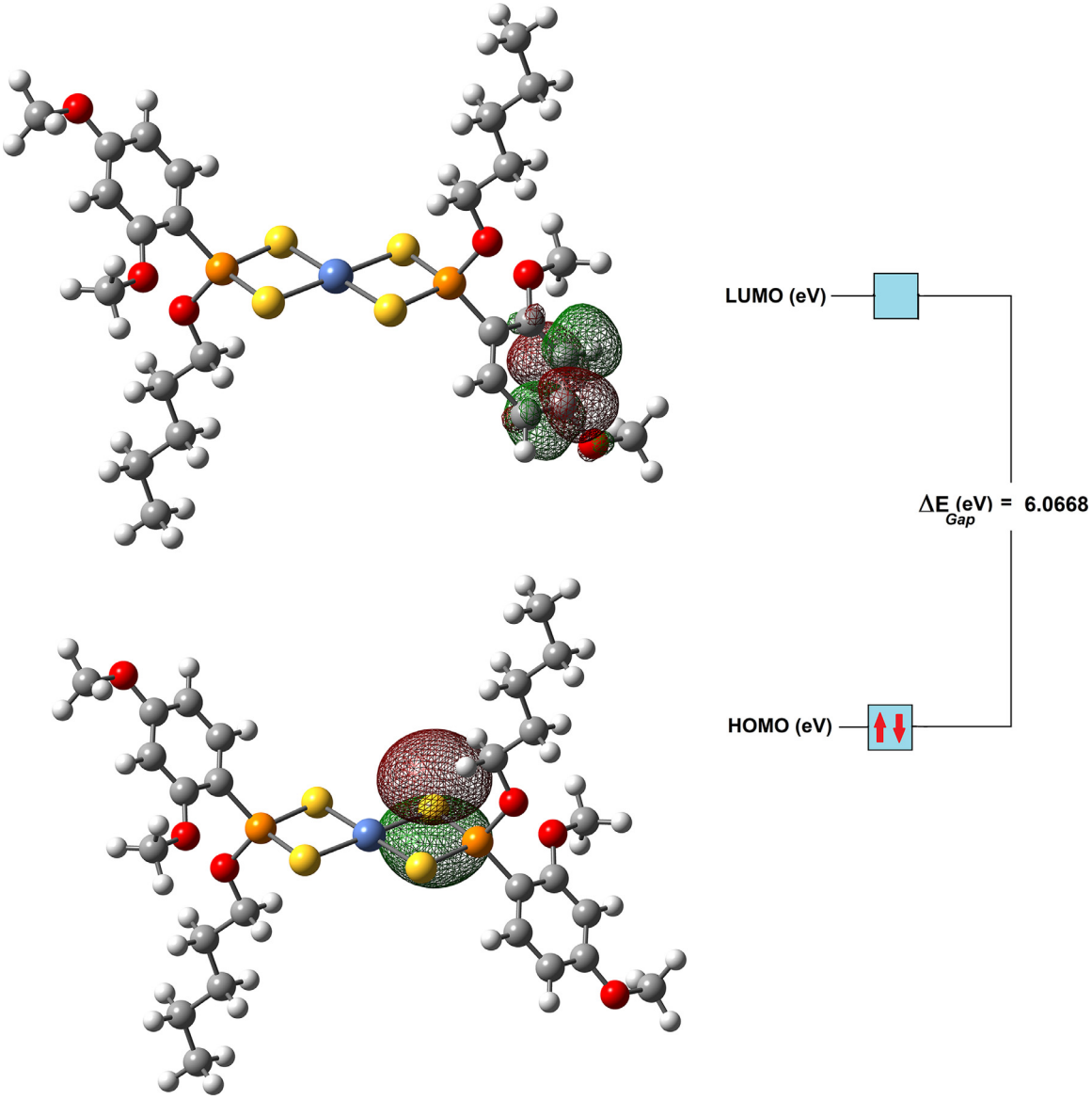

Fig. 6. HOMO and LUMO electron density isosurfaces and band gap values (eV) of the complex $[Ni(L2)_2]$.

As a general pattern, NMR (^{1}H, ^{13}C and ^{31}P) signals of the complexes are displayed at higher fields relative to those observed for the corresponding ligands. All the NMR data are reasonably consistent with the literature reports for similar structures [46–52].

The unambiguous assignments of ^{1}H and ^{13}C NMR data of $[Ni(L2)_2]$ complex was dealt with by using HSQC spectra (Fig. 2). According to HSQC two-dimensional NMR spectrum data, the positions of $\boldsymbol{C}_2$, $\boldsymbol{C}_3$ and $\boldsymbol{C}_5$ atoms in the 2,4-dimethoxyphenyl ring confirm the expected structure, as well as in single-crystal X-ray study.

3.2. Description of crystal structure and optimized molecular structure of $[Ni(L2)_2]$

The crystal structure of $[Ni(L2)_2]$ was unambiguously elucidated through single-crystal X-ray diffraction analysis to better understand its solid-state structure (Fig. 3A). $[Ni(L2)_2]$ crystallizes in the triclinic crystal system with *P*-1 with the asymmetric unit consisting of one Ni(II) cation and one ligand (L2). The Ni(II) ion is located on a crystallographic inversion center. The dihedral an-

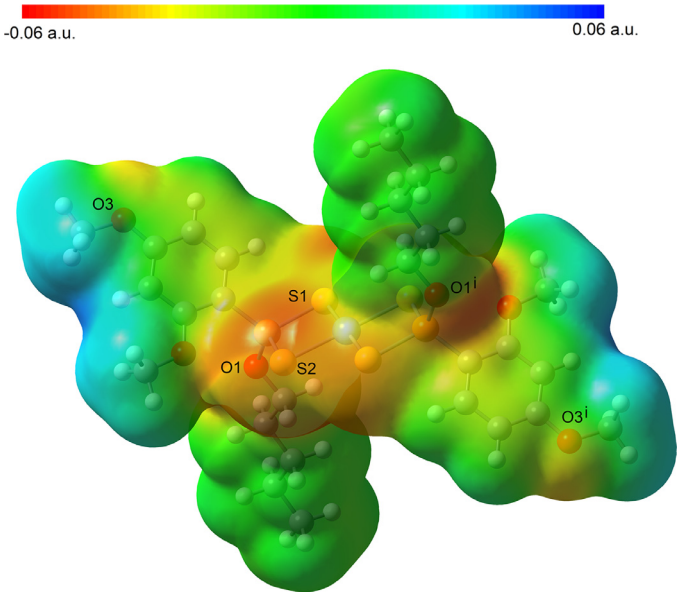

Fig. 7. Molecular electrostatic potential (MEP) surfaces for the complex $[Ni(L2)_2]$.

gle between the 2,4-dimethoxyphenyl ring and NiS_4 coordination plane in the complex is 61.83° and also the dithiophosphonate moieties are in trans arrangement with respect to the coordination plane. The Ni metal center has a square planar coordination geometry by four sulfur atoms (S1, $S1^i$, S2, $S2^i$) from two dithiophosphonate ligands, forming four-membered chelate rings with an S1—Ni1—S2 angle of 87.929(15)°, and these angles agree with those observed in related Ni(II) complexes (CSD. Ref. Code: NORFUV, RIVQUI, RIVRAP) [53,54]. The Ni—S bond distances (Ni1—S1 = 2.2216(5) Å and Ni1—S2 = 2.2412(5) Å) are in the normal ranges and are well-matched to those found in Ni(II) complexes (CSD Ref. Code: XORKAT, DUKMIH, HAHDAW, LIGFAJ, NIRMAF, NORFUV) [53,55-59]. The P1—S1 and P1—S2 bond lengths are 2.0036(6) Å and 2.0093(6) Å, respectively, are intermediate between the P—S (~2.1 Å) and $P = S$ (~1.90 Å) bond distances, which reflect that π-electron delocalization prevails in the $-PS_2$ of dithiophosphonate moiety. Unsurprisingly, the 2D fingerprint plots (Fig. 4A) exhibit that the most effective contact in solid-state of $[Ni(L2)_2]$ is the H/H interaction contributing to the total Hirshfeld surface with the value equal to 54.5% owing to the plentiful hydrogen atoms through aliphatic side groups. The weak C—H···O (C8-H8C···O1, (d(C8···O1) = 3.347 Å; C7—H7C···O3, (d(C7···O3) = 3.325 Å, Table 5) hydrogen bonding interactions link the molecules to form 2D hydrogen-bonded layers (Fig. 3C). The resulting 2D layers are further expanded into a 3D supramolecular network through C11—H11A···S1 (d(C11···S1) = 3.347 Å) interactions, forming the hydrogen bonding rings with R2,2(18) motif, as shown in Fig. 3D. HS of $[Ni(L2)_2]$ are illustrated in Fig. 3B and the O···H/ H···O and S···H/ H···S interactions constitute 13% and 17.3%, respectively, appearing as distinct spikes in the 2D fingerprint plot (Fig. 4A). The closest C—H···π phenyl (d(H···π)) = 2.77 Å, Table 5) interaction is illustrated in the shape index-mapped Hirshfeld surfaces (Fig. 4B) and also help to stabilize the crystal structure of $[Ni(L2)_2]$. On the other hand, the curvedness mapped on the HS (Fig. 4B) does not show a large flat region, which reflects no important $\pi-\pi$ stacking interactions less than π phenyl···π phenyl < 3.8 Å.

The optimized 3D structural parameters of the investigated complex $[Ni(L2)_2]$ were calculated using B3LYP/LANL2DZ/6–31+G(d,p) level in the ground state. The optimized molecular figure of the complex is given in Fig. 5. Experimental and theoretical values of selected bond lengths and angles were listed in Table 6.

3.3. Hirshfeld surface (HS) analysis

HS [60] incorporating 2D fingerprint plots [61] using Crystal Explorer [62] program was used in order to get a better insight into

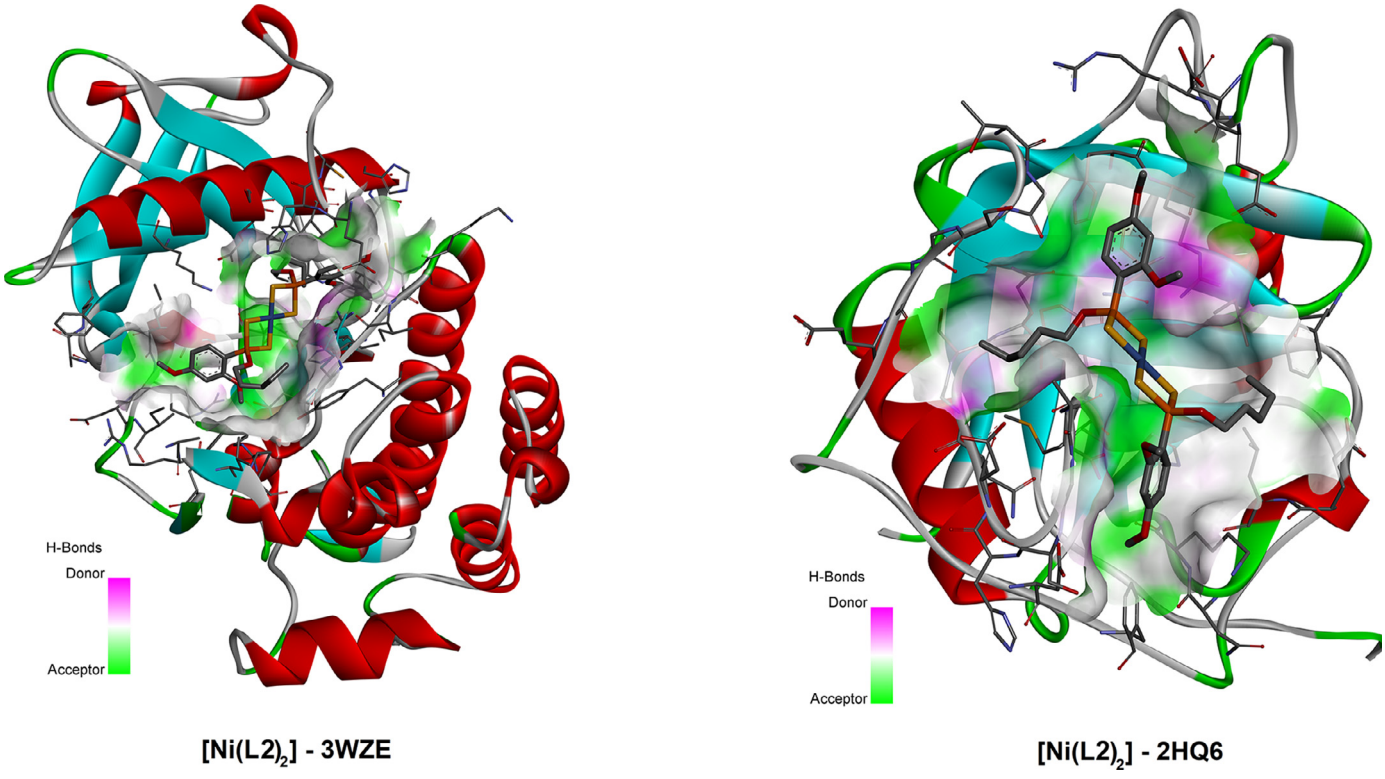

Fig. 8. Energetically most favorable docked poses were obtained from the rigid molecular docking of $[Ni(L2)_2]$ with 3WZE and 2HQ6.

Table 8
Binding interactions of the compounds [Ni(L2)$_2$] with liver cancer protein, PDB ID: 3WZE and colon cancer antigen proteins, PDB ID: 2HQ6.

Compound (UNK0)−3WZE and 2HQ6	Name	Distance (Å)	Bonding types (Category and binding mode)(H: Hydrogen; HB: Hydrogen Bond; HFB: Hydrophobic)
[Ni(L2)$_2$] - 3WZE	UNK0:S - A:ASP1046:OD2	3.6139	Conventional Hydrogen Bond (H) [D2-O···S2i]
	UNK0:S - A:ASP1046:OD2	3.4770	Conventional Hydrogen Bond (H) [D2-O···S1]
	UNK0:S - A:HIS1026:O	3.1366	Conventional Hydrogen Bond (H) [C–O···S2i]
	UNK0 - A:ILE1053	5.2295	Pi-Alkyl (HFB) [π orbitals → Alkyl]
	A:TYR1082 - UNK0:C	4.0834	Pi-Alkyl (HFB) [π orbitals → Alkyl]
	A:ARG1027:NH1 - UNK0	3.7277	Pi-Cation (HFB) [H1-N → π orbitals]
	A:CYS1024:SG - UNK0	5.0079	Pi-Sulfur (Other) [G-S → π orbitals]
	A:ILE888:CD1 - UNK0	3.8076	Pi-Sigma (HFB) [C–H → π orbitals]
	UNK0:C - A:LEU889	5.2759	Alkyl (HFB) [Alkyl → Alkyl]
	UNK0:C - A:GLU815:O	3.3808	Carbon Hydrogen Bond (HB) [C–H···O]
[Ni(L2)$_2$] - 2HQ6	A:ARG56:NH1 - UNK0:S	3.0786	Conventional Hydrogen Bond (H) [H1-N···S1]
	A:GLN64:NE2 - UNK0:O	3.1482	Conventional Hydrogen Bond (H) [E2-N···O1]
	UNK0 - A:LYS126	4.9857	Pi-Alkyl (HFB) [π orbitals → Alkyl]
	A:PHE61 - UNK0:C	5.0052	Pi-Alkyl (HFB) [π orbitals → Alkyl]
	UNK0 - A:ARG56	4.9188	Pi-Alkyl (HFB) [π orbitals → Alkyl]
	UNK0:C - A:LEU123	4.9040	Alkyl (HFB) [Alkyl → Alkyl]
	UNK0:S - A:HIS127	5.9748	Pi-Sulfur (Other) [S → π orbitals]
	UNK0:S - A:HIS127	4.6153	Pi-Sulfur (Other) [S → π orbitals]
	A:ARG56:NH1 - UNK0	4.0069	Pi-Cation (HFB) [H1-N → π orbitals]
	UNK0:Ni - A:ASN103:O	2.7925	Metal-acceptor (Metal) [Ni → O]
	UNK0:C - A:SER106:OG	3.7505	Carbon Hydrogen Bond (HB) [C–H···O]
	UNK0:C - A:ASP152:O	3.5472	Carbon Hydrogen Bond (HB) [C–H···O]
	UNK0:C - A:LYS126:O	3.5429	Carbon Hydrogen Bond (HB) [C–H···O]

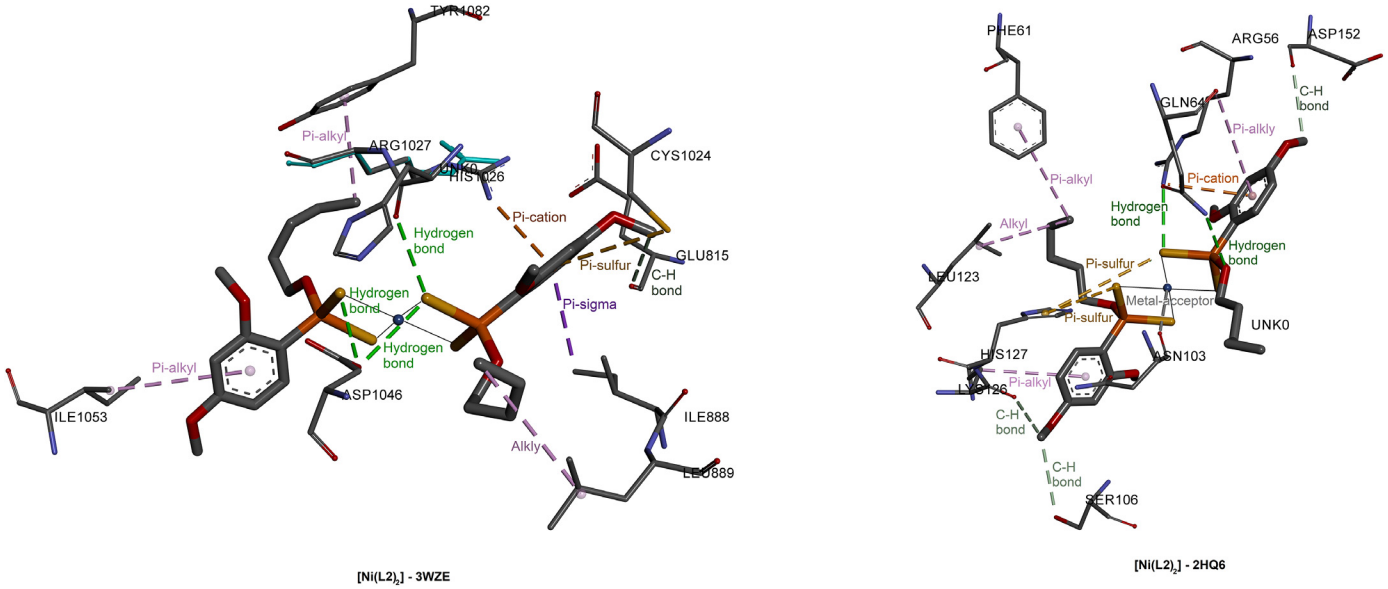

Fig. 9. The non-covalent interactions of [Ni(L2)$_2$] with 3WZE and 2HQ6.

Table 9
IC_{50} results for compounds against cancer cell lines.

Compounds	IC_{50} (μM)	
	DLD-1	HepG2
[NH_4L1]	>200	>200
[NH_4L2]	>200	>200
[NH_4L3]	127.50	>200
[Ni(L1)$_2$]	131.40	>200
[Ni(L2)$_2$]	>200	>200
[Ni(L3)$_2$]	**65.67**	>200
Cisplatin	48.83	31.91

the intermolecular interactions in the solid-state of [Ni(L2)$_2$]. The normalized contact distance (d_{norm}) surface, which is expressed in terms of distances to the surface from the nuclei inside and outside the HS (d_i, and d_e, respectively) and the vdW radii of the atoms, defined as Eq. (1) gives the identification of the regions of particular importance to intermolecular interactions [59,63]. The 2D fingerprint plots, which were derived from the combination of d_i, and d_e, were used for quantifying the intermolecular contacts in the crystal.

$$d_{norm} = \frac{d_i - r_i^{vdw}}{r_i^{vdw}} + \frac{d_e - r_e^{vdw}}{r_e^{vdw}} \quad (1)$$

The resolved fingerprint plots showing the percentage contributions to the total HS (HS) area in [Ni(L2)$_2$] are given in Fig. 4A.

3.4. Computational methods

3.4.1. Frontier orbitals and chemical parameters of [Ni(L2)$_2$]

Frontier orbitals (HOMOs and LUMOs) are very important for chemical reactivity and are associated with electron affinity and

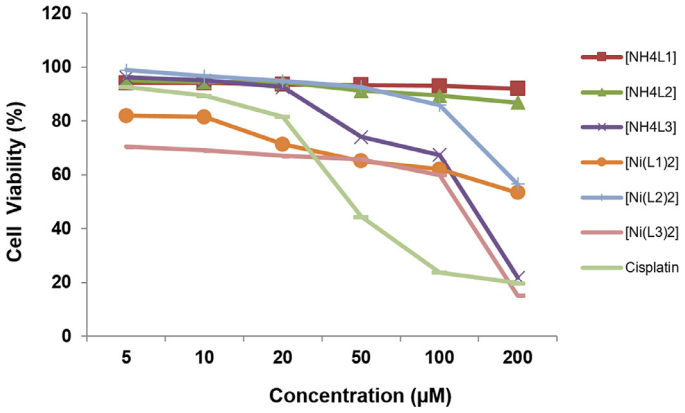

Fig. 10. Antiproliferative effect of compounds on DLD-1 cells.

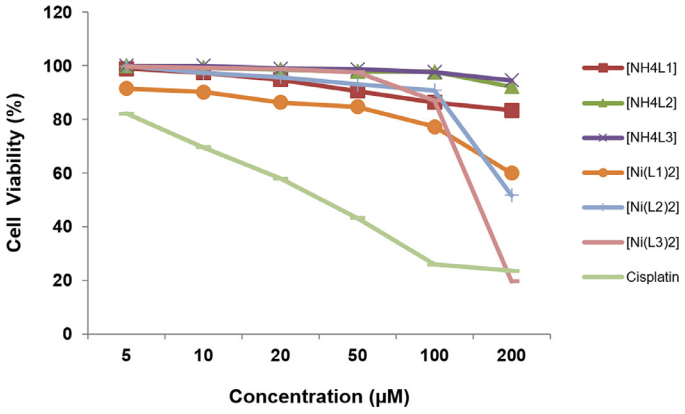

Fig. 11. Antiproliferative effect of compounds on HepG2 cells.

ionization potential. According to Koopmans theorem [10], chemical parameters such as ionization potential (*IP*), electron affinity (*EA*), chemical hardness (η), absolute electronegativity (χ) and absolute softness (σ) can be calculated if the energy values of the frontier orbitals are determined.

The energy gap, $\Delta E_{Gap} = (E_{LUMO} - E_{HOMO})$, between HOMO and LUMO makes it easy to predict the chemical and electrical properties of molecules. Thus, to determine the chemical parameters of $[Ni(L2)_2]$, the energy gaps between HOMOs and LUMOs were calculated with the B3LYP/LANL2DZ/6–31+*G*(d,p) level of the DFT in the ground state. The total energies, calculated chemical parameters and energy gaps $\Delta E_{Gap} = (E_{LUMO} - E_{HOMO})$ of $[Ni(L2)_2]$ were given in Table 7. As seen in Table 7, the value of ΔE_{Gap} is 6.0668 eV in the gas phase. The energy levels and configurations of HOMO and LUMO are shown in Fig. 6. HOMO is mainly localized on the $S2^i$ atom of the 2,4-dimethoxyphenyl ring, while LUMO is mainly only localized on the phenyl group in $[Ni(L2)_2]$ (Fig. 6). The low energy gap value has a significant effect on the intermolecular charge transfer and bioactivity of the molecule. The low energy gap ΔE_{Gap} value has a significant influence on the intermolecular charge transfer and bioactivity of the molecule.

3.4.2. The MEP surfaces of the complex $[Ni(L2)_2]$

Electrostatic potential maps (MEPs) are very useful 3D diagrams for visualizing charge distributions of molecules. They are valuable tools for describing the charge-related properties and to visualize the size and shape of molecules. Thus, the non-covalent interactions predicted by MEPs can be a lead to predict the charge transfer and bioactivity centers of the molecule. In MEPs, negative regions colored in red exhibit higher electron density (electrophilic reactivity), while positive regions colored blue exhibit low electron density (nucleophilic reactivity). To determine the electrophilic and nucleophilic reactivity of $[Ni(L2)_2]$, MEP surfaces were determined and visualized with B3LYP/LANL2DZ/6–31+*G*(d,p) level using Gaussian 09 and Gauss-view visualization programs. The diagram of MEP was illustrated in Fig. 7. The maximum electron density (electrophilic reactivity) values of O1 ($O1^i$), O3 ($O3^i$), S1 ($S1^i$) and S2 ($S2^i$) atoms from the MEP diagram of $[Ni(L2)_2]$ were calculated as 0.0519, 0.0355, 0.0425 and 0.0510 a.u. The maximum positive region value is 0.0465 a.u. and the positive region indicating nucleophilic reactivity are shown in the MEP diagrams in Fig. 7. These regions provide preliminary information to predict intermolecular interactions.

3.4.3. Molecular docking studies

Molecular docking studies can be used to model interactions between molecules and a target protein at the atomic level. These models serve in drug discovery and development studies and save time, thereby providing low costs. The molecular docking studies of $[Ni(L2)_2]$ were done with liver cancer protein, PDB ID: 3WZE and colon cancer antigen proteins, ID 2HQ6. The bonding energies and RMSD values for each molecular docking study of the investigated compounds are listed comparatively in Table 2. Energetically most favorable docked poses obtained from the rigid molecular docking of each compound with 3WZE and 2HQ6 were illustrated in Fig. 8. The binding sites, binding types and bond distances are given in Table 8 according to the molecular docking studies of the compounds. The non-covalent interactions of $[Ni(L2)_2]$ with 3WZE and 2HQ6 using the molecular docking study were revealed and illustrated as 3D in Fig. 9. The relative binding energy values are −7.3 and −6.0 kcal/mol docked with investigated Ni(II) complex and liver cancer protein (PDB ID: 3WZE) and colon cancer antigen proteins (PDB ID: 2HQ6), respectively.

The molecular docking results indicate that nine amino acids, namely, ASP1046, HIS1026, ILE1053, TYR1082, ARG1027, CYS1024, ILE888, LEU889, and GLU815 of the liver cancer protein (PDB ID: 3WZE) are found to interact with $[Ni(L2)_2]$ complex. The predicted non-covalent interactions are of types: three conventional hydrogen bonds, one carbon-involving hydrogen bond, two (pi-system)-alkyl interaction, one (pi-system)-sigma bond, one (pi-system)-cation, one (pi-system)-sulfur and one alkyl interactions. The conventional hydrogen bond lengths are 3.137 (between the O oxygen atom on HIS1026 and S2i atom of dithiophosphonato-complex); 3.477 Å (between the OD2 oxygen on ASP1046 and S2i atom of dithiophosphonato-complex) and 3.614 Å (between the OD2 oxygen on ASP1046 and S1 atom of dithiophosphonato-complex).

Docking studies also show that ten different amino acids ARG56, GLN64, LYS126, PHE61, LEU123, HIS127, SER106, ASP152 LYS126 and ASN103 of colon cancer antigen proteins (PDB ID: 2HQ6) interact with the $[Ni(L2)_2]$ complex. The non-covalent interactions are: two conventional hydrogen bonds, three carbon-involving hydrogen bonds, one (pi-system)-cation bond, three (pi-system)-alkyl, two (pi-system)-sulfur, one metal acceptor and alkyl interactions. The conventional hydrogen bond lengths are 3.079 Å (between NH1 nitrogen on ARG56 and S1 atom of dithiophosphonato-complex), 3.148 Å (between NE2 nitrogen on GLN64 and O1 atom of the *n*-pentyl group in dithiophosphonato-complex).

3.5. Cytotoxic activity studies of compounds as in vitro

The antiproliferative activity of ligands and their nickel complexes were tested at different concentrations against liver and colon human cancer cell lines for 48 h. The results are given in Table 9.

The tested $[NH_4Ln]$ and $[Ni(Ln)_2]$ (n = 1–3) exhibited IC_{50} values in the ranges of values 65.67 and >200 μM in the human

colon adenocarcinoma cell line (DLD-1). According to this made structure-activity relationship (SAR) study, substituents on the molecule structures certainly have a significant effect on DLD-1. For example, one of the Ni complexes [Ni(L3)$_2$] containing 4–*tert*–but-benzyl group showed a very effective result with 65.67 μM compared to the other compounds in DLD-1, and this value is very close to the IC_{50} value obtained from the positive control drug cisplatin. On the other hand, the complex [Ni(L3)$_2$] exhibited nearly two times higher cytotoxic activity than other synthesized compounds in the DLD-1 cell line. At the same time, the ligand [Ni(L3)$_2$] of this metal complex [NH_4L3] demonstrated higher antiproliferative activity on the DLD-1 cell line compared to the other two ligands [NH_4L1] and [NH_4L2] with IC_{50} value of 127.50 μM. This clearly shows that the substituents on the structure affect the activity of the molecule. Complex [Ni(L1)$_2$] with IC_{50} value of 131.40 μM, had moderate toxic effect on the inhibition of colon cancer cell growth as *in vitro*. However, compounds [NH_4L1], [NH_4L2] and [Ni(L2)$_2$] were found to be inactive towards DLD-1 for the tested concentrations and incubation time.

We also evaluated *in vitro* antiproliferative activity of compounds towards the HepG2 cell line. Interestingly, all tested compounds were found to be inactive in this cell line. Even, the most effective complex [Ni(L3)$_2$] in the DLD-1 cell line was found to have an IC_{50} value higher than 200 μM in HepG2. The variation of the antiproliferative effect of the compounds on cells for 48 h depending on the concentrations is given in Figs. 10 and 11.

As seen in Fig. 10, the compounds [NH_4L3], [Ni(L1)$_2$]-[Ni(L3)$_2$] tested inhibited the proliferation of dividing colon and liver cancer cells in a dose-dependent manner. However, compounds [NH_4L1] and [NH_4L2] did not show any effect on cell viability ratio even at a concentration as high such as 200 μM. The viability ratios of DLD-1 cells were obtained in 93.48%, 94.25%, 92.49%, 71.27%, 94.78%, 66.99% and 81.54% at 20 μM concentration of [NH_4Ln], [Ni(Ln)$_2$] and (n = 1–3) and cisplatin, respectively. When the concentrations of tested compounds were increased to 200 μM, the viability ratio of DLD-1 cells changed as follows: 91.89%, 86.76%, 21.78%, 53.25%, 56.47%, 15.13%, 19.68% for [NH_4Ln], [Ni(Ln)$_2$] (n = 1–3) and cisplatin, respectively. The results show that the ligand [NH_4L3] and its metal complex have a significant toxic effect on DLD-1 at 200 μM concentration and greatly inhibit cell growth.

The synthesized ligands and complexes generally do not effect on liver cancer cells growth. The viability ratios of HepG2 cells were obtained in 83.40%, 92.19%, 94.55%, 59.93%, 51.65%, 19.62%, 23.52% at 200 μM concentration of [NH_4Ln], [Ni(Ln)$_2$] (n = 1–3) and cisplatin, respectively. When 100 μM of complex [Ni(L3)$_2$] was used, the cell viability ratio was measured as 87.13%. This ratio was dramatically reduced to 19.62% with 200 μM of the same complex. However, there was no significant change in liver cancer cell inhibition with the concentration change of the other compounds (Fig. 11).

4. Conclusion

A new intermediate dithiophosphorus compound, 2,4-*bis*(2,4-dimethoxyphenyl)−1,3-dithia-2,4-diphosphetane 2,4-disulfide was prepared to use in the synthesis of a series of ditihophosphonic acids ammonium salts, [NH_4Ln] and the corresponding Ni(II) complexes, [Ni(Ln)$_2$]. This intermediate is meant to enrich the new route of synthesis we have developed by using 2,4-*bis*(3-methoxytolyl)−1,3-dithia-2,4-diphosphetane 2,4-disulfide (SAV-B1), 2,4-*bis*(2-methoxytolyl)−1,3-dithia-2,4-diphosphetane 2,4-disulfide (SAV-B2) [26] and 2,4-*bis*(3,4-dimethoxyphenyl)−1,3-dithia-2,4-diphosphetane 2,4-disulfide, (SAV-A1) [64]. The new intermediate 2,4-*bis*(2,4-dimethoxyphenyl)−1,3-dithia-2,4-diphosphetane 2,4-disulfide will be coded SAV-A2. The codes are given to emphasize that the four intermediates are the continuation of an integral effort to facilitate easy routes for the synthesis of dithio-phosphorus compounds.

The DFT calculations of [Ni(L2)$_2$] were presented. Calculated structural parameters of the Ni complexes were compared with the molecular structures obtained from X-ray analysis by using DFT. Total molecular energies, the energy values of HOMO-LUMO band gaps, the chemical parameters, the HOMO and LUMO diagrams and MEP analysis of the complexes were reported by the quantum mechanical calculations. Energetically most favorable docked poses were also obtained from the rigid molecular docking of investigated Ni complex with liver cancer protein, PDB ID: 3WZE and colon cancer antigen proteins, ID 2HQ6. The binding sites, binding types and bond distances are predicted by molecular docking studies of the compounds.

The compounds were screened in human cell lines, and it was found that some compounds have toxic effect. In particular, a complex [Ni(L3)$_2$] was found to be more effective than the others with an IC_{50} value of 65.67 μM in DLD-1.

Declaration of Competing Interest

The authors declare that they have no known competing financial interests or personal relationships that could have appeared to influence the work reported in this work.

CRediT authorship contribution statement

Ertuğrul Gazi Sağlam: Conceptualization, Validation, Formal analysis, Investigation, Resources, Supervision, Writing – original draft, Writing – review & editing, Visualization, Funding acquisition. **Elif Bulat:** Conceptualization, Visualization, Methodology, Formal analysis, Investigation, Writing – original draft, Visualization, Funding acquisition. **Celal Tuğrul Zeyrek:** Software, Resources, Writing – original draft, Formal analysis, Formal analysis, Investigation, Visualization. **Senem Akkoç:** Validation, Investigation, Resources, Writing – original draft, Visualization. **Yunus Zorlu:** Software, Formal analysis, Resources, Validation, Investigation, Writing – original draft, Visualization. **Hamza Yılmaz:** Validation, Writing – original draft, Writing – review & editing.

Data Availability

No data was used for the research described in the article.

Acknowledgements

This work was supported by the Project Coordination Application and Research Center of Marmara University [FDK-2021–10339]. Anticancer studies were also supported by Suleyman Demirel University Research Fund for financial support with project number TSG-2021–8458. The numerical calculations reported in this paper were fully/partially performed at TUBITAK (The Scientific and Technological Research Council of Turkey; ULAKBIM), High Performance and Grid Computing Center (TRUBA resources).

Supplementary materials

Supplementary material associated with this article can be found, in the online version, at doi:10.1016/j.molstruc.2022.134197.

References

[1] N Tercero, DR Nagaraj, R Farinato, A critical overview of dithiophosphinate and dithiophosphate interactions with base metal sulfides and precious metals, Min. Metall. Explor. 36 (2019) 99–110, doi:10.1007/s42461-018-0039-1.

[2] D Kim, TJ Toops, K Nguyen, MJ Lance, J Qu, Impact of primary and secondary ZDDP and ionic liquid as lubricant oil additives on the performance and physicochemical properties of pd-based three-way catalysts, Catalysts 11 (8) (2021) 878, doi:10.3390/catal11080878.

[3] AV Artem'ev, SF Malysheva, NK Gusarova, NA Belogorlova, SV Fedorov, BV Timokhin, VI Smirnov, BA Trofimov, Novel quinine, lupinine, and anabasine derivatives containing dithiophosphinate groups, Chem Heterocycl Compd (N Y) 48 (3) (2012) 448–452, doi:10.1007/s10593-012-1013-3.

[4] RT Delfino, TS Ribeiro, JD Figueroa-Villar, Organophosphorus compounds as chemical warfare agents: a review, J. Braz. Chem. Soc. 20 (3) (2009) 407–428, doi:10.1590/S0103-50532009000300003.

[5] BD Durckheimer W, E Ehlers , Schrinner E, Heymes R, Cephem Derivates, 1988.

[6] C Socaciu, I Pasca, C Silvestru, A Bara, I Haiduc, Antitumor organometallics. IV. The mutagenic potential of some diphenylantimony(III) dithiophosphorus derivatives, Met-Based Drugs 1 (1994) 237030, doi:10.1155/MBD.1994.291a.

[7] BK Keppler, C Silvestru, I Haiduc, Antitumour organometallics. III. in vivo activity of diphenylantimony(III) and diorganotin(IV) dithiophosphorus derivatives against P_{388} leukemia, Met. Based Drugs 1 (1994) 73–77, doi:10.1155/MBD.1994.73.

[8] B Brian C. Froehler, CA, Hydrogen phosphonodithioate compositions, US 5,194,599 A (1993).

[9] B Brian C. Froehler, CA, 2004, Nucleoside hydrogen phosphonodithioate diesters and activated phosphonodithioate analogues, US 6,756,496 B1 (2004).

[10] W Feng, XY Teo, W Novera, PM Ramanujulu, D Liang, DJ Huang, PK Moore, LW Deng, BW Dymock, Discovery of new H_2S releasing phosphorodithioates and 2,3-dihydro-2-phenyl-2-sulfanylenebenzo[d] [1,3,2]oxazaphospholes with improved antiproliferative activity, J. Med. Chem 58 (2015) 6456–6480, doi:10.1021/acs.jmedchem.5b00848.

[11] X-b Yang, Methods and compositions of improved modified siRNA, US 2015/0322 431 A1 (2015).

[12] A Lowe, Whittaker, M, Dieterich, P, Polywka, M, Cossimino, E, Dithiophosphato-Platinum-Complexes for The Treatment of Cancer, WO 2005/095425 A1 (2005).

[13] S Kumar, A Syed, S Andotra, R Kaur, Vikas, SK Pandey, Investigation of synthesized new vanadium(III) complexes of ditolyldithiophosphate ligands by spectroscopic, cyclic voltammetric, DFT, antimicrobial and cytotoxic studies, J. Mol. Struct. 1154 (2018) 165–178, doi:10.1016/j.molstruc.2017.10.009.

[14] M Karakus, H Yilmaz, E Bulak, P Lönnecke, Bis{μ-[O-*cyclopentyl*(4-*methoxyphenyl*) *dithiophosphonato*]1κ:s,2κ:s-[O-*cyclopentyl*(4-*methoxyphenyl*) *dithiophosphonato*]1κ^2S,S'} dizinc(II), Appl. Organometal. Chem. 19 (3) (2005) 396–397, doi:10.1002/aoc.850.

[15] I Haiduc, 1.15 - 1,1-Dithiolato Ligands, in: J.A. McCleverty, T.J. Meyer (Eds.), Comprehensive Coordination Chemistry II, 2003, pp. 349–376. Pergamon, Oxford.

[16] WE van Zyl, JD Woollins, The coordination chemistry of dithiophosphonates: an emerging and versatile ligand class, Coordin. Chem. Rev. 257 (2013) 718–731, doi:10.1016/j.ccr.2012.10.010.

[17] TL Yusuf, TW Quadri, GF Tolufashe, LO Olasunkanmi, EE Ebenso, WE van Zyl, Synthesis and structures of divalent Co, Ni, Zn and Cd complexes of mixed dichalcogen and dipnictogen ligands with corrosion inhibition properties: experimental and computational studies, RSC Adv. 10 (69) (2020) 41967–41982, doi:10.1039/D0RA07770D.

[18] TL Yusuf, CU Ibeji, WE van Zyl, Nickel(II) complexes from phosphordichalcogenide (P/Se_2 and P/S_2) type ligands: synthesis, structure and theoretical calculations, J. Mol. Struct. 1218 (2020) 128517, doi:10.1016/j.molstruc.2020.128517.

[19] M Karakus, H Yilmaz, Synthesis and characterization of Ni(II), Zn(II), and Cd(II) complexes with dithiophosphonate derivatives, Russian J. Coordin. Chem. 32 (6) (2006) 437–443, doi:10.1134/S1070328406060078.

[20] K Diemert, W Kuchen, Zur kenntnis der organophosphorverbindungen, XVII1 dithiophosphinsäuren RR'P(S)SH, ihre synthese, derivate und metallkomplexe, Phosphorus, Sulfur, Relat. Elem. 3 (2) (1977) 131–136, doi:10.1080/03086647708077702.

[21] CK Thomsen I, S Scheibye, Thiation with 2,4-bis(4-methoxyphenyl)-1,3,2,4-dithiadiphosphetane 2,4-disulfide: n-methylthiopyrrolidone, lawesson S-O, Org. Synth. 62 (1984) 158, doi:10.15227/orgsyn.062.0158.

[22] G Lajoie, F Lépine, L Maziak, B Belleau, Facile regioselective formation of thiopeptide linkages from oligopeptides with new thionation reagents, Tetrahedron Lett. 224 (36) (1983) 3815–3818, doi:10.1016/S0040-4039(00)94282-5.

[23] P Wipf, C Jenny, H Heimgartner, 2,4-Bis(4-methylpheylthio)-1,3,2λ^5,4λ^5-dithiadiphosphetan-2,4-dithion: ein neues reagens zur schwefelung von N,N-disubstituierten Amiden, Helv. Chim. Acta 70 (4) (1987) 1001–1011, doi:10.1002/hlca.19870700412.

[24] MRSJ Foreman, AMZ Slawin, JD Woollins, 2,4-diferrocenyl-1,3-dithiadiphosphetane 2,4-disulfide; structure and reactions with catechols And [$PtCl_2(PR_3)_2$](R = Et or Bun), J. Chem. Soc., Dalton Trans. (18) (1996) 3653–3657, doi:10.1039/DT9960003653.

[25] M Yokoyama, Y Hasegawa, H Hatanaka, Y Kawazoe, T Imamoto, Improved O/S exchange reagents, Synthesis 1984 (10) (1984) 827–829, doi:10.1055/s-1984-30980.

[26] EG Sağlam, E Bulat, H Yılmaz, The syntheses and characterization of new dithiophosphonates derived from Novel 2,4-Bis(methoxytolyl)-1,3-dithia-2,4-diphosphetane 2,4-disulfides and Their Ni(II) complexes, JOTCSA 7 (2020) 789–800, doi:10.18596/jotcsa.773478.

[27] APEX2, Version 2014.11-0, Bruker (2014), Bruker AXS Inc., Madison, WI (2014).

[28] VA SAINT, Bruker (2013), Bruker AXS Inc., Madison, WI,, (2014).

[29] V SADABS, Bruker (2014), Bruker AXS Inc., Madison, WI, (2014).

[30] G Sheldrick, SHELXT - Integrated space-group and crystal-structure determination, Acta Cryst. A 71 (1) (2015) 3–8, doi:10.1107/S2053273314026370.

[31] G Sheldrick, Crystal structure refinement with SHELXL, Acta Cryst. C 71 (1) (2015) 3–8, doi:10.1107/S2053229614024218.

[32] OV Dolomanov, LJ Bourhis, RJ Gildea, JAK Howard, H Puschmann, OLEX2: a complete structure solution, refinement and analysis program, J. Appl. Cryst. 42 (2) (2009) 339–341, doi:10.1107/S0021889808042726.

[33] A Spek, Structure validation in chemical crystallography, Acta Cryst. D 65 (2) (2009) 148–155, doi:10.1107/S090744490804362X.

[34] CF Macrae, PR Edgington, P McCabe, E Pidcock, GP Shields, R Taylor, M Towler, J van de Streek, Mercury: visualization and analysis of crystal structures, J. Appl. Cryst. 39 (3) (2006) 453–457, doi:10.1107/S002188980600731X.

[35] TKR Dennington, J Millam, in: S.M. KS (Ed.) GaussView, Semichem, Inc. 2009.

[36] IHFSTH Dunning Jr., PJ Hay, Methods of Electronic Structure Theory, Gaussian Basis Sets For Molecular Calculations, Springer, 1977.

[37] AD Becke, Density-functional thermochemistry. IV. A new dynamical correlation functional and implications for exact-exchange mixing, J. Chem. Phys. 104 (3) (1996) 1040–1046, doi:10.1063/1.470829.

[38] J-P Blaudeau, MP McGrath, LA Curtiss, L Radom, Extension of gaussian-2 (G2) theory to molecules containing third-row atoms K and Ca, J. Chem. Phys. 107 (13) (1997) 5016–5021, doi:10.1063/1.474865.

[39] O Trott, AJ Olson, AutoDock Vina: improving the speed and accuracy of docking with a new scoring function, efficient optimization, and multithreading, J. Comput. Chem. 31 (2) (2010) 455–461, doi:10.1002/jcc.21334.

[40] DSB Corp., Discovery Studio Visualizer Software, 2015.

[41] News & Views, J. Mol. Graphics Mod. 17 (1) (1999) 55–84, doi:10.1016/S1093-3263(99)99999-0.

[42] B Kramer, M Rarey, T Lengauer, Evaluation of the FLEXX incremental construction algorithm for protein–ligand docking, Proteins: Structure, Function, and Bioinformatics 37 (2) (1999) 228–241 doi:10.1002/(SICI)1097-0134(19991101)37:2≤228::AID-PROT8≥3.0.CO;2-8.

[43] AB Gurung, MA Ali, A Bhattacharjee, M AbulFarah, F Al-Hemaid, FM Abou-Tarboush, KM Al-Anazi, FS Al-Anazi, J Lee, Molecular docking of the anticancer bioactive compound proceraside with macromolecules involved in the cell cycle and DNA replication, Genet. Mol. Res. 15 (2) (2016), doi:10.4238/gmr.15027829.

[44] S Akkoç, Derivatives of 1-(2-(Piperidin-1-yl)ethyl)-1H-benzo[*d*]imidazole: synthesis, characterization, determining of electronic properties and cytotoxicity studies, ChemistrySelect 4 (17) (2019) 4938–4943, doi:10.1002/slct.201900353.

[45] S Akkoç, Antiproliferative activities of 2-hydroxyethyl substituted benzimidazolium salts and their palladium complexes against human cancerous cell lines, Synth Commun 49 (21) (2019) 2903–2914, doi:10.1080/00397911.2019.1650187.

[46] TJ Ajayi, M Shapi, Solvent-free mechanochemical synthesis, hirshfeld surface analysis, crystal structure, spectroscopic characterization and NBO analysis of Bis(ammonium) Bis((4-methoxyphenyl) phosphonodithioato)-nickel (II) dihydrate with DFT studies, J. Mol. Struct. 1202 (2020) 127254, doi:10.1016/j.molstruc.2019.127254.

[47] M Karakus, H Yilmaz, Y Ozcan, S Ide, Crystallographic report: bis{μ-[O-*cyclopentyl*(4-*methoxyphenyl*)*dithiophosphonato*]1κ:s,2κ:s-[O-*cyclopentyl*(4-*methoxyphenyl*)*dithiophosphonato*]-1κ^2S,S'}dicadmium(II), Appl. Organometal. Chem. 18 (3) (2004) 141–142, doi:10.1002/aoc.588.

[48] H Beckmann, G Ohms, G Großmann, K Krüger, K Klostermann, V Kaiser, Synthesis, crystal structure, and NMR spectroscopy of a 1,3,2λ^5,4λ^5-oxathiadiphosphetane, Heteroatom Chemistry 7 (2) (1996) 111–118 doi:10.1002/(SICI)1098-1071(199603)7:2≤111::AID-HC2≥3.0.CO;2-G.

[49] G Grossmann, H Beckmann, O Rademacher, K Krüger, G Ohms, Crystal structure, nuclear magnetic resonance spectroscopy and individual gauge for localised orbitals (IGLO) calculations of $C_6H_4P_2S_6$, a new tetrathiadiphosphorinane, and comparison with related P–S compounds, J. Chem. Soc., Dalton Trans. (17) (1995) 2797–2803, doi:10.1039/DT9950002797.

[50] G Kallinowski, W Vogt, ^{13}C nuclear magnetic resonance study of some phosphinolipids: assignments and conformational studies, Magn. Reson. Chem. 27 (7) (1989) 647–652, doi:10.1002/mrc.1260270708.

[51] JJMA Al-Rawi, MA Sheat, N Ayed, Carbon-13 NMR of some organophosphorus compounds. 2 chemical shifts and P-C coupling constants of diaryl-, dialkoxy- and diaryloxy-phosphine amines with general formula Y_2PNRR', Org. Magn. Reson. 22 (5) (1984) 336–339, doi:10.1002/mrc.1270220512.

[52] GA Gray, Carbon-13 nuclear magnetic resonance of organophosphorus compounds. I. Diethyl phosphonates, J. Am. Chem. Soc. 93 (9) (1971) 2132–2140, doi:10.1021/ja00738a007.

[53] M Arca, A Cornia, FA Devillanova, AC Fabretti, F Isaia, V Lippolis, G Verani, New perspectives in phosphonodithioate coordination chemistry. Synthesis and X-ray crystal structure of trans-bis-[O-ethyl-(4-methoxyphenyl)phosphonodithioato] nickel(II), Inorg. Chim. Acta 262 (1) (1997) 81–84, doi:10.1016/S0020-1693(97)05491-1.

[54] MC Aragoni, M Arca, F Demartin, FA Devillanova, C Graiff, F Isaia, V Lippolis, A Tiripicchio, G Verani, Reactivity of phosphonodithioato NiII complexes: solution equilibria, solid state studies and theoretical calculations on the adduct formation with some pyridine derivatives, Dalton Trans. (18) (2001) 2671–2677, doi:10.1039/B100991P.

[55] TJ Ajayi, M Ollengo, L le Roux, MN Pillay, RJ Staples, SM Biros, K Wenderich, B Mei, WE van Zyl, Heterodimetallic ferrocenyl dithiophosphonate complexes of nickel(II), zinc(II) and cadmium(II) as sensitizers for TiO_2-based dye-sensitized solar cells, ChemistrySelect 4 (25) (2019) 7416–7424, doi:10.1002/slct.201900622.

[56] EG Sağlam, A Ebinç, CT Zeyrek, H Ünver, T Hökelek, Structural studies on some dithiophosphonato complexes of Ni(II), Cd(II), Hg(II) and theoretical studies on a dithiophosphonato Ni(II) complex using density functional theory, J. Mol. Struct. 1099 (2015) 490–501, doi:10.1016/j.molstruc.2015.06.087.
[57] IP Gray, AMZ Slawin, JD Woollins, Synthesis and structure of $[An(RO)PS_2]^-$ complexes, Dalton Trans (16) (2004) 2477–2486, doi:10.1039/B406411A.
[58] W Shi, R Kelting, M Shafaei-Fallah, A Rothenberger, Transformations of P-chalcogenide precursors with a hydrated metal salt, J. Organomet. Chem. 692 (13) (2007) 2678–2682, doi:10.1016/j.jorganchem.2006.11.009.
[59] JJ McKinnon, D Jayatilaka, MA Spackman, Towards quantitative analysis of intermolecular interactions with Hirshfeld surfaces, Chem. Commun. (37) (2007) 3814–3816, doi:10.1039/B704980C.
[60] MA Spackman, D Jayatilaka, Hirshfeld surface analysis, CrystEngComm 11 (1) (2009) 19–32, doi:10.1039/B818330A.
[61] MA Spackman, JJ McKinnon, Fingerprinting intermolecular interactions in molecular crystals, CrystEngComm 4 (66) (2002) 378–392, doi:10.1039/B203191B.
[62] MJ Turner, JJ McKinnon, SK Wolff, DJ Grimwood, PR Spackman, D Jayatilaka, MA Spackman, CrystalExplorer17, University of Western Australia, 2017.
[63] JJ McKinnon, MA Spackman, AS Mitchell, Novel tools for visualizing and exploring intermolecular interactions in molecular crystals, Acta Cryst. B 60 (6) (2004) 627–668, doi:10.1107/S0108768104020300.
[64] E Bulat, EG Sağlam, CT Zeyrek, S Akkoç, Y Zorlu, H Dal, Ni(II) complexes with 1,3,2,4-dithiadiphosphetane 2,4-disulfide-based ligands: structural insights, theoretical studies, and anticancer activities, Appl. Organomet. Chem. B e6821 (2022) 1–23, doi:10.1002/aoc.6821.